Bridge Structures, Vol. 1, No. 3, September 2005, 133–168

Taylor & Francis
Taylor & Francis Group

State-of-the-art in cable vibrations of cable-stayed bridges

MICHEL VIRLOGEUX

Consulting Engineer and Designer, Bonnelles, France

This paper presents a simplified view of cable vibrations in cable-stayed bridges. The different types of cable vibrations are described with an emphasis on parametric excitation which is more of a structural than aerodynamic problem. Countermeasures to eliminate or reduce cable vibrations are discussed with examples of cable vibrations.

Keywords: Cable-stayed bridges; Cable vibrations; Vortex shedding; Wake effects; Buffeting; Aerodynamic stability; Parametric excitation; Rain- and wind-induced vibrations; Cross cables

1. Introduction

Significant progress has been made in bridge aerodynamics during the last two decades. That includes theoretical approaches, wind tunnel tests, and computer software development for the evaluation of structural response. On one hand, bridge engineers have better understanding of bridge aerodynamic stability as well as dynamic response to turbulent wind. On the other hand, this understanding is used to maintain unsuitable shapes for long-span cable-stayed bridges, such as steel I-girders or prestressed concrete rectangular ribs, for economy. A better alternative is to develop more stream-lined profiles.

More attention has been given to cable vibrations, observed for the first time in 1977 in the Brotonne Bridge in France (figures 1 and 2). While the controversial phenomenon of vibrations in cable-stayed bridges could have been easily stopped with the installation of hydraulic dampers, many other cable-stayed bridges suffered from similar cable vibrations. These include Ben Ahin and Wandre Bridges in Belgium, Faro and Oresund Bridges in Denmark, Glebe Island Bridge in Australia, the Second Severn Crossing in the UK, Erasmus Bridge in Rotterdam, the Burlington Bridge in the United States, and several bridges in Japan. It appeared that many different phenomena can generate cable vibrations. Thorough research studies were performed in many countries and the cable vibration phenomenon is now well understood.

The need for a solution to the vibration problem intensified in light of recent breakage in stay cables at the Saint-Nazaire bridge in France (figures 3–5), and Zarate Brazo Largo bridge in Argentina. It is the author's opinion that these breaks are due to fatigue induced by cable vibrations.

In this paper, the problem of cable vibrations is handled from the designer's point of view. The main reason for this approach is the lack of sound theories, and the gap that exists between sophisticated theories and design practices. It is therefore necessary to generate simplified models that are readily accessible to a wider base of cable-stayed bridge designers. Thus, this paper adopts a direct language to evoke opinions regarding the issues that ought to be considered in the analysis of cable vibrations, which developed in some bridges. The paper aims at an honest presentation of the issues associated with cable vibrations in cable-stayed bridges.

2. Statics of stay cables

2.1 *Linear analysis*

In the classical computations performed for the structural analysis of cable-stayed bridges, each stay cable is modelled as a straight elastic member between its two anchorages, A and B (figure 6). The cable length is L, the horizontal distance between anchorages is ℓ, and the vertical distance is h. The angle between the stay cable and the horizontal is α, where:

$$\mathrm{tg}\alpha = \frac{h}{\ell}$$

*Fax: +(33) 13088-4344

Bridge Structures
ISSN 1573-2487 print/ISSN 1744-8999 online © 2005 Taylor & Francis
http://www.tandf.co.uk/journals
DOI: 10.1080/15732480500301004

Figure 1. The Brotonne Bridge.

Figure 2. Stay cables of the Brotonne Bridge when vibrating during construction (photo courtesy of J. Combault).

Figure 3. The Saint-Nazaire Bridge.

Figure 4. Broken stay cable (32 downstream) at the Saint-Nazaire Bridge.

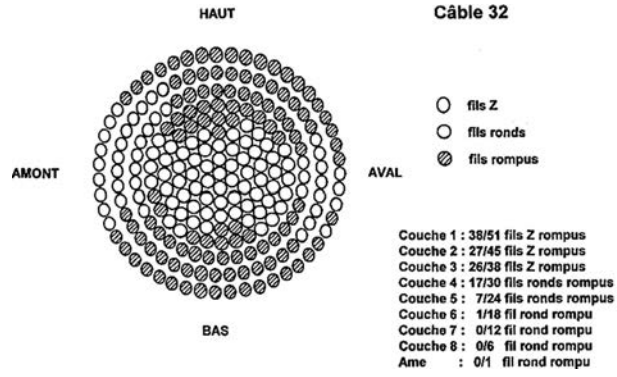

Figure 5. Distribution of broken wires at the Saint-Nazaire Bridge; stay cable 32 downstream.

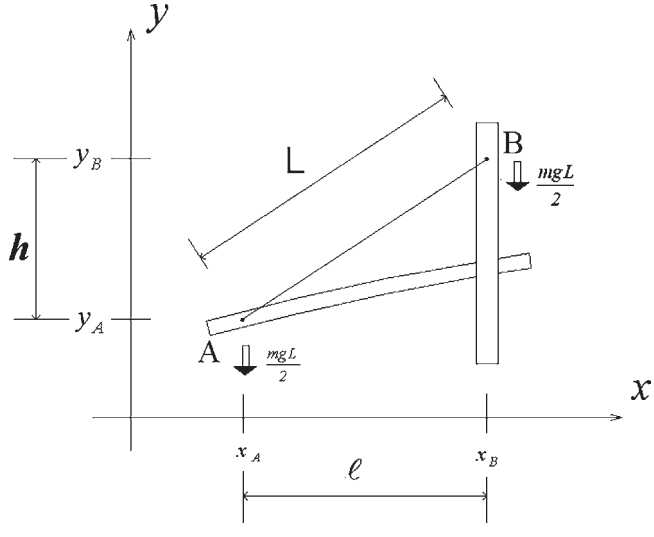

Figure 6. Model of a stay cable for linear structural analysis.

The weight of the stay cable ($mg\,L$), where m is the lineic mass, is introduced, evenly, at the anchorages A and B. The tension in the stay cable, resulting from the analysis, is denoted as F. The result is only accurate under permanent loads if the computations have been performed with a value of the modulus of elasticity corresponding to the sag effect in the stay cable for this load case, as shown later.

2.2 *The catenary*

If the weight of the stay cable is distributed along its length, the tension varies along the cable. The basic equations are given by the equilibrium of a differential cable segment (figure 7). Considering horizontal forces, the horizontal projection of the cable tension is constant, and is given by H:

$$H = F(x)\,\cos\theta(x) \tag{1}$$

Vertical forces give the differential equation:

$$F(x+\mathrm{d}x)\sin\theta(x+\mathrm{d}x) - F(x)\sin\theta(x) = mg\,\mathrm{d}s = mg\sqrt{1+y'(x)^2}\,\mathrm{d}x$$

Using equation (1), one obtains the following differential equation:

$$H\frac{\mathrm{d}^2y}{\mathrm{d}x^2} = mg\sqrt{1+y'(x)^2}$$

This leads to the classical catenary shape, given by:

$$y(x) = y_0 + \frac{H}{mg}ch\left(\frac{mg}{H}(x-x_0)\right)$$

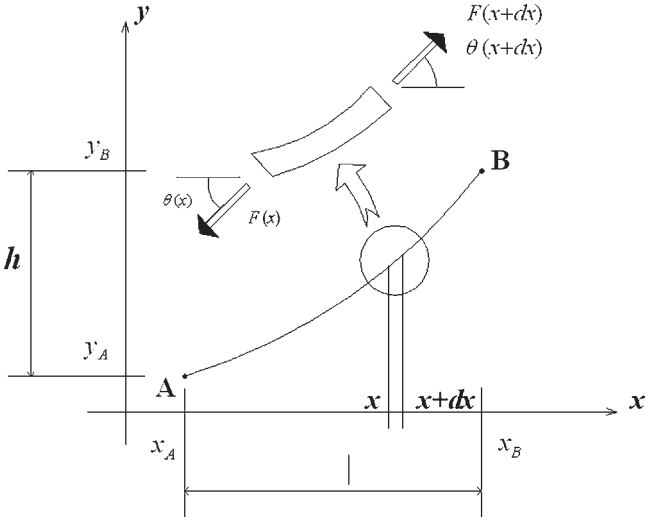

Figure 7. Static equilibrium of a catenary cable segment.

The parameters, x_0 and y_0, are given by the two anchorage points, A and B. The first parameter, x_0, is given by:

$$x_0 = \frac{x_A + x_B}{2} - \frac{H}{mg}\mathrm{Arg}\,sh\left[\frac{mg(y_B - y_A)}{2H\,sh\left(\frac{mg(x_B - x_A)}{2H}\right)}\right] = \frac{(x_A + x_B)}{2} - \frac{H}{mg}\mathrm{Arg}\,sh\left[\frac{mgh}{2H\,sh\left(\frac{mg\ell}{2H}\right)}\right]$$

When noting:

$$K = \mathrm{Arg}\,sh\left[\frac{mgh}{2H\,sh\left(\frac{mg\ell}{H}\right)}\right] - \frac{mg(x_A + x_B)}{2H} \tag{2}$$

the catenary equation can be written as:

$$y(x) = \frac{H}{mg}\left[ch\left(\frac{mg}{H}x + K\right) - ch\left(\frac{mg}{H}x_A + K\right)\right] + y_A \tag{3}$$

The vertical distance between the catenary stay cable and the chord is given by:

$$f_v(x) = \frac{h}{\ell}(x - x_A) - \frac{H}{mg}\left[ch\left(\frac{mg}{H}x + K\right) - ch\left(\frac{mg}{H}x_A + K\right)\right] \tag{4}$$

It is maximum for:

$$sh\left(\frac{mg}{H}x + K\right) = \frac{h}{\ell}$$

that is for:

$$x_m = \frac{x_A + x_B}{2} + \frac{H}{mg}\left[\mathrm{Arg}\,sh\left(\frac{h}{\ell}\right) - \mathrm{Arg}\,sh\left(\frac{mgh}{2H\,sh\left(\frac{mg\ell}{2H}\right)}\right)\right] \tag{5}$$

Many results can be derived from this model, including the value of the apparent modulus of elasticity of the stay cable, corresponding to the relation between the increase in tension and the increase in the distance, L, between the anchorages produced by loads imposed on the structure.

2.3 *Simplified approach*

The extreme vertical sag, which can be precisely evaluated from equations (4) and (5), can be estimated with a good accuracy from the equilibrium of the lower part of the cable, between the lower anchorage and mid-span, C, supposing that the catenary cable is parallel to the chord at mid-span (figure 8). The resulting moment at A, produced by the tension at mid-span, F, and by the weight of the cable has to be equal to zero:

$$Ff_v\cos\alpha = mg\frac{L}{2}x\frac{L\cos\alpha}{4}$$

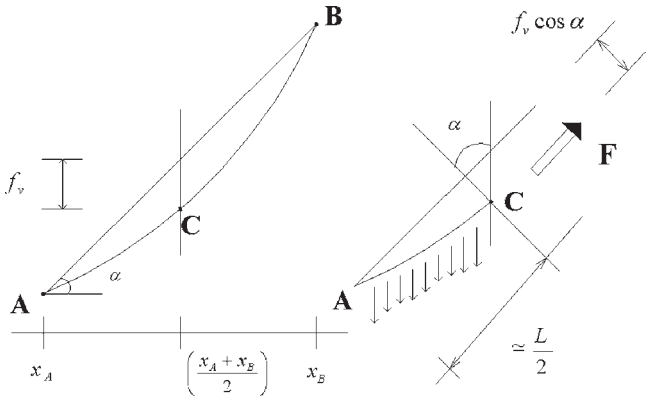

Figure 8. Definition of stay cable vertical sag.

Thus

$$f_v \approx \frac{mgL^2}{8F} \tag{6}$$

The equilibrium of vertical forces, when analysed at both anchorages and at mid-span, gives:

$$\begin{aligned} F_A \sin\theta_A &= F\sin\alpha - \frac{mgL}{2} \\ F_B \sin\theta_B &= F\sin\alpha + \frac{mgL}{2} \end{aligned} \tag{7}$$

This relation demonstrates that the tension at mid-span can be identified with the result of a classical linear analysis as described above; thus:

$$H = F\cos\alpha \tag{8}$$

3. Dynamics of stay cables

3.1 *Simplified analysis of natural frequencies*

The classical evaluation of cables natural frequencies is based on a simple model, which considers the cable with a constant tension F. The equation which governs the vibration is given by the dynamic equilibrium of a differential segment of cable (figure 9):

$$m\,\mathrm{d}x\frac{\mathrm{d}^2y}{\mathrm{d}t^2} = F\frac{\mathrm{d}^2y}{\mathrm{d}x^2}\mathrm{d}x + f(x,t)\mathrm{d}x$$

where $f(x,t)$ is the lineic external force produced on the stay cable at the abscise x, perpendicular to the stay cable, for example by the wind. This leads to the equation:

$$m\frac{\mathrm{d}^2y}{\mathrm{d}t^2} - F\frac{\mathrm{d}^2y}{\mathrm{d}x^2} = f(x,t) \tag{9}$$

The solution for equation (9) is obtained by separating the variables, x and t. This can be achieved by using the classical mode shapes written as follows:

$$y(x,t) = \sum_{i=1}^{n} \sin\left(\frac{i\pi x}{L}\right) y_i(t) \tag{10}$$

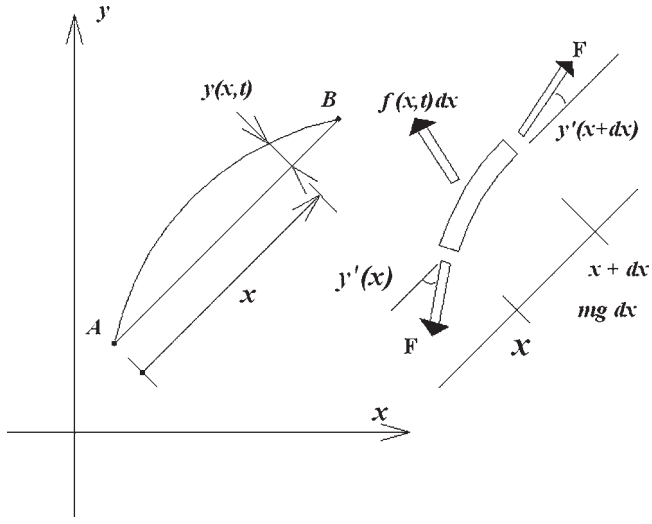

Figure 9. Dynamic equilibrium of a stay cable segment.

Thus:

$$\sum_{i=1}^{n}\left[m\sin\left(\frac{i\pi x}{L}\right)y_i''(t) + F\left(\frac{i\pi}{L}\right)^2\sin\left(\frac{i\pi x}{L}\right)y_i(t)\right] = f(x,t)$$

Multiplying by $\sin(k\pi x/L)$, an integration between 0 and L gives:

$$\sum_{i=1}^{n}\left[m\,y_i''(t) + F\left(\frac{i\pi}{L}\right)^2 y_i(t)\right]\int_0^L \sin\left(\frac{k\pi x}{L}\right)\sin\left(\frac{i\pi x}{L}\right)\mathrm{d}x = \int_0^L \sin\left(\frac{k\pi x}{L}\right) f(x,t)\mathrm{d}x$$

where

$$\int_0^L \sin\left(\frac{k\pi x}{L}\right)\sin\left(\frac{i\pi x}{L}\right)\mathrm{d}x = 0 \quad \forall i \neq k \quad \text{and} \quad \int_0^L \left[\sin\left(\frac{k\pi x}{L}\right)\right]^2\mathrm{d}x = \frac{L}{2}$$

The dynamic equation for mode k becomes:

$$y_k''(t) + \left(\frac{k\pi}{L}\right)^2\frac{F}{m}y_k(t) = \frac{2}{mL}\int_0^L f(x,t)\sin\left(\frac{k\pi x}{L}\right)\mathrm{d}x \tag{11}$$

The pulsation for mode k is given by:

$$\omega_k = \frac{k\pi}{L}\sqrt{\frac{F}{m}} \tag{12}$$

and thus the period is given by:

$$T_k = \frac{2L}{k}\sqrt{\frac{m}{F}} \tag{13}$$

The generalised external force is expressed by:

$$f_k(t) = \frac{2}{mL}\int_0^L f(x,t)\sin\left(\frac{k\pi x}{L}\right)\mathrm{d}x \tag{14}$$

Adding damping to equation (11) results in the following form:

$$y_k''(t) + 2\omega_k\xi_k y_k'(t) + \omega_k^2 y_k(t) = f_k(t) \tag{15}$$

where ξ_k is the damping coefficient in mode k (ratio to critical).

These results are valid for all transverse vibrations of stay cables, as well as 'vertical' (in the vertical plane of the stay cable) or 'lateral' (perpendicular to the vertical plane of the stay cable).

3.2 *Forces produced in the deck by cable vibrations*

It is necessary to understand the influence of a stay cable vibration on the deck. As the cable sag has an influence at least on the first mode, one has to approach its shape with a sinusoidal formula, as follows:

$$y_0(x) = -f\sin\left(\frac{\pi x}{L}\right)$$

where f, the transverse sag, shown in figure 10, is given by: $f = f_v\cos\alpha$.

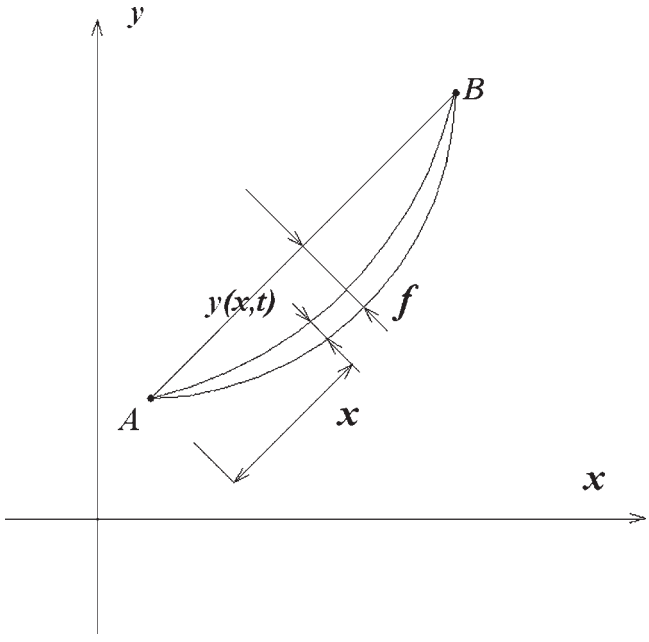

Figure 10. Definition of the vibration from equilibrium with the sag effect.

The cable vibration on mode k is given from its equilibrium position by:

$$y(x,t) = A_k\sin\left(\frac{k\pi x}{L}\right)\sin(\omega_k t)$$

The derivate of the above relationship is given by:

$$y'(x,t) = \frac{k\pi}{L}A_k\cos\left(\frac{k\pi x}{L}\right)\sin(\omega_k t)$$

whereas the distance from the chord is written as:

$$d(x,t) = A_k\sin\left(\frac{k\pi x}{L}\right)\sin(\omega_k t) - f\sin\left(\frac{\pi x}{L}\right)$$

The cable vibration has two effects. First, it produces a change in the cable inclination at its lower anchorage (for $x = 0$), changing the vertical effect of the cable tension on the deck:

$$\Delta V = \frac{k\pi\ell}{L^2}FA_k\sin(\omega_k t) \tag{16}$$

In addition, it produces a length variation which is given by:

$$\Delta L = \int_0^L\sqrt{1+[y'(x,t)]^2}\,\mathrm{d}x - \int_0^L\sqrt{1+[y_0'(x)]^2}\,\mathrm{d}x$$

A first-order approximation for the length variation, for all modes $k > 1$, is:

$$\Delta L = \frac{k\pi^2(A_k\sin(\omega_k t))^2}{4L} \tag{17}$$

whereas, for $k = 1$, the length variation is given by:

$$\Delta L = \frac{\pi^2}{4L}\left(A_1^2\sin^2(\omega_k t) - 2A_1 f\sin(\omega_k t)\right) \tag{18}$$

The vibration corresponds to a shortening when the cable moves upwards, and to an extension when it moves downwards. In all situations, the length variation produces a tension variation and from there a variation in the cable vertical action on the deck. The resulting global variation in the vertical cable action on the deck, for any mode k greater than one, is given by:

$$\Delta V = \frac{k\pi\ell}{L^2}FA_k\sin(\omega_k t) + \frac{k\pi^2 h}{4L^3}ESA_k^2\left(\frac{1-\cos(2\omega_k t)}{2}\right) \tag{19}$$

where E is the modulus of elasticity of the cable, and S is the area of its cross section.

It can be seen that the first term, which corresponds to the change in the cable inclination, varies with the same pulsations ω_k as the cable vibrates. The second term, which comes from the length variation, varies with a pulsation $2\omega_k$, that is, with a period which is only half the period of the cable vibration. There is a critical value of the

amplitude, independent from the order k, below which the first term is predominant, and above which the second term is more important. The critical value of the amplitude, A_{kcr}, is given by:

$$A_{kcr} = \frac{4L\ell}{\pi h}\frac{F}{ES} \tag{20}$$

At the Erasmus Bridge in Rotterdam, the critical amplitude of cable vibration is 0.68 m for cable 10 and 1.00 m for cable 13. These values are higher than the reasonable values for mode 2 and above. The same example can give an idea of practical forces; for mode 2 and an amplitude of 0.50 m, the extreme vertical force on the deck (combining the two terms) is 42 kN for cable 10 and 35 kN for cable 13.

For mode one ($k = 1$), the resulting vertical action is slightly different, where:

$$\Delta V = \left[\frac{\pi\ell}{L^2}F - \frac{\pi^2 h}{2L^3}ESf\right]A_1\sin(\omega_1 t) + \frac{\pi^2 h}{4L^3}ESA_1^2\left(\frac{1-\cos(2\omega_1 t)}{2}\right) \tag{21}$$

Once again, one term varies with the same frequency as the cable vibration, but a part of it also comes from the effects of length variations, while the other one has half of the period. An amplitude of 1.0 m at the Erasmus Bridge produced an extreme vertical force of 127 kN for cable 10 and 109 kN for cable 13. These results show that significant cable vibrations can produce high vertical lift forces on the deck, to the extent of exciting structural vibrations. It is worth noting that uncorrelated vibrations of different cables cannot have significant effects. In other words, cable vibrations must be correlated to produce a significant excitation in the whole structure.

3.3 *Work to produce the extreme transverse displacement*

To evaluate the work, ΔW, which is transferred to the stay cable, from the equilibrium position, $y_0(x)$, to the situation corresponding to the extreme upwards deflection for any mode k, $y(x)$, one writes:

$$y_0(x) = -f\sin\left(\frac{\pi x}{L}\right)$$

$$y(x) = A_k\sin\left(\frac{k\pi x}{L}\right)$$

The amount of work is given by:

$$\Delta W = \Delta W_{int} - \Delta W_{ext}$$

where ΔW^{int} is the deformation work of the cable produced by its elongation, and ΔW^{ext} is the work of the external forces limited to the cable weight. The deformation work is evaluated by:

$$\Delta W_{int} = F\Delta L + \frac{1}{2}\Delta F\Delta L = F\Delta L + \frac{1}{2}\frac{ES}{L}\Delta L^2$$

For any mode k the external work is given by:

$$\Delta W_{ext} = -\int_0^L A_k\sin\left(\frac{k\pi x}{L}\right)mg\cos\alpha\,dx = -\frac{2mgL\cos\alpha}{k\pi}\delta_k A_k$$

where δ_k is equal to zero when k is even (2, 4, 6, ...) and is equal to one when k is uneven (1, 3, 5, ...).

According to equation (17), for a mode k greater than one, when the extreme amplitude is reached:

$$\Delta L = \frac{k\pi^2 A_k^2}{4L}$$

Thus the global work is given by:

$$\Delta W = \frac{2mgL\cos\alpha}{k\pi}\delta_k A_k + \frac{k\pi^2 F}{4L}A_k^2 + \frac{1}{2}\frac{ES}{L}\left(\frac{k\pi^2}{4L}\right)^2 A_k^4 \tag{22}$$

It is clear that the existence of a factor with A_k for uneven modes (3, 5, 7, ...) is incorrect and just shows that sag effects still have some influence on the vibrations for these modes.

For the first mode, using equation (18), when the amplitude is extreme:

$$\Delta L = -\frac{\pi\left(2fA_1 - A_1^2\right)}{4L}$$

so that the global work can be written as:

$$\Delta W = \frac{2mgL\cos\alpha}{\pi}A_1 - \frac{\pi^2 F}{4L}\left(2fA_1 - A_1^2\right) + \frac{1}{2}\frac{ES}{L}\left(\frac{\pi^2}{4L}\right)^2\left(2fA_1 - A_1^2\right)^2$$

since one cannot have a factor A_1, the sag, f, is given by:

$$f = \frac{4mgL^2\cos\alpha}{\pi^3 F}$$

This is not much different from the previous estimate, derived from equation (6):

$$f \approx \frac{mgL^2\cos\alpha}{8F}, \quad \text{with } \frac{\pi^3}{4} = 7.7516 \approx 8$$

One can conclude that the expression

$$\Delta W = \frac{\pi^2 F}{4L}A_1^2 + \frac{1}{2}\frac{ES}{L}\left(\frac{\pi^2}{4L}\right)^2\left(2fA_1 - A_1^2\right)^2 \tag{23}$$

is a good approximation of the work.

3.4 *More precise approach of the first natural frequency*

Consider again a cable vibrating vertically in the first mode, with sag effects. Its typical position is given by:

$$y(x,t) = \sin\left(\frac{\pi x}{L}\right)[A_1 \sin \omega_1 t - f]$$

where the velocity is expressed by:

$$v(x,t) = A_1\omega_1 \sin\left(\frac{\pi x}{L}\right)\cos \omega_1 t$$

The equation of the kinetic energy between the equilibrium position, where the cable has its extreme velocity

$$v(x) = A_1\omega_1 \sin\left(\frac{\pi x}{L}\right)$$

and the extreme upwards position where the velocity decreases to zero, is limited to:

$$\Delta W_{\text{ext}} = \Delta C + \Delta W_{\text{int}}$$

Rearranging the above relationship results in the following expression:

$$-\Delta C = \Delta W_{\text{int}} - \Delta W_{\text{ext}} = \Delta W$$

The above is another form of equation (23). Since the variation of the kinetic energy can be written:

$$\Delta C = -\frac{1}{2}\int_0^L m\left(A_1\omega_1 \sin\left(\frac{\pi x}{L}\right)\right)^2 \mathrm{d}x = -\frac{\omega_1^2 mL}{4}A_1^2,$$

re-using equation (23), the equation of the kinetic energy renders:

$$\frac{\omega_1^2 mL}{4}A_1^2 = \frac{\pi^2 F}{4L}A_1^2 + \frac{1}{2}\frac{ES}{L}\left(\frac{\pi^2}{4L}\right)^2 (2fA_1 - A_1^2)^2$$

The identification of the terms of the second order (A_1^2) gives an evaluation of ω_1:

$$\omega_1^2 = \frac{\pi^2 F}{mL^2} + \frac{ES}{mL^2}\frac{\pi^2}{2L^2}f^2$$

The period, T_1, is given by:

$$T_1 = 2L\sqrt{\frac{m}{F\left(1 + \frac{ES}{F}\frac{\pi^2 f^2}{2L^2}\right)}} \tag{24}$$

The results given by equation (24) were compared to those computed by the traditional evaluation, using equation (13), and also with the finite element analysis performed by for the longer cable of the Normandie Bridge (Morisset and Riché 1994), for two different values of the cable tension. Table 1 demonstrates the accuracy of the evaluation by equation (24), in seconds, compared with the finite element analysis and equation (13), which is still valid for lateral vibrations.

4. Aerodynamic forces on stay cables

4.1 *Drag coefficient of cable ducts*

The drag force on a cable is given by:

$$F_d = \frac{1}{2}\rho U^2 D C_d \tag{25}$$

where ρ is the air density (1.23 kg m^{-3}), U is the wind velocity, D is the cable diameter and C_d is the drag coefficient. For a classical cylinder, the coefficient is high for the small values of the wind velocity, or the Reynolds number, which is given by

$$R_e = \frac{UD}{v} \tag{26}$$

where v is the air viscosity equal to 15×10^{-6} in the MKSA system; the drag coefficient is equal to about 1.20 in this undercritical domain. For a critical value of the Reynolds number which varies between 2×10^5 and 5×10^5, depending on the duct rugosity, the drag coefficient drops down to about 0.60 or 0.50 in the domain of the overcritical values of the Reynolds number, and even lower. For higher values of the Reynolds number, the drag coefficient increases and reaches a stable value in the hypercritical domain which depends on the duct rugosity (figure 11). Classical stay

Table 1. Comparison of the evaluation of the first vertical vibration period, in seconds, by three methods.

Method of analysis	F = 260 kN	F = 4090 kN
Computation (A. Morisset and Ch. Riché 1994)	3.63	3.43
Evaluation (equation (24))	3.632	3.432
Traditional evaluation (equation (13))	4.600	4.133

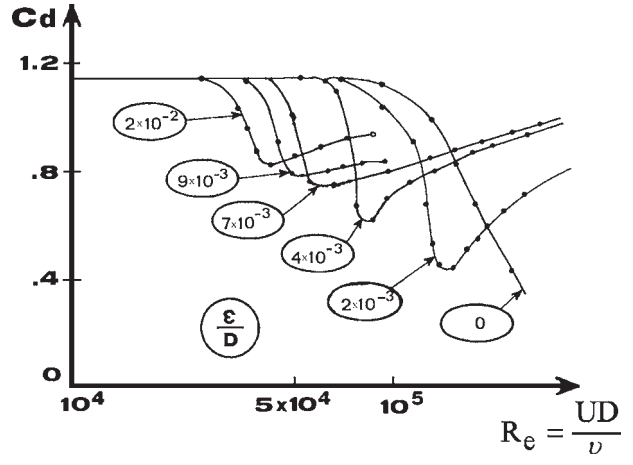

Figure 11. The drag coefficient of a classical duct as a function of the Reynolds number and of the duct rugosity (from CSTB).

cables are generally in the overcritical domain for extreme winds, but the drag coefficient may increase for more frequent winds, around 10 m s^{-1}, which may be in the undercritical or critical domain. Wind forces are frequently computed with a value of 0.70 (or even 0.80 in very conservative analyses) to cover uncertainties due to the evolution of rugosity with time. For the Normandie Bridge, the author evaluated the global effects with a value of 0.65 considering that all cables could not be in unfavourable conditions at the same time (Virlogeux 1992). It should be noted that drag forces on stay cables are of more significance for long-span cable-stayed bridges, as the wind forces on the deck are reduced to very low values by an efficient streamlining. For instance, about 55% of the horizontal bending moment (vertical axis) in the box-girder superstructure of the Normandie Bridge, at its connections to the pylons, were produced by wind forces on stay cables and only 45% by wind forces on the box-girder itself (Virlogeux 1996). Modern stay cables are confined in ducts, or pipes, which receive some shaping designed to reduce the risk of rain and wind-induced cable vibrations as will be demonstrated later in this paper. This shaping evidently influences drag effects and has to be considered.

Figure 12 shows the first shaped pipe in high-density polyethylene (HDPE), provided with longitudinal ribs to channel water downwards. It has been installed on the Higashi-Kobe Bridge, in Japan. The deep channels increased the drag coefficient of a classical cylinder from 0.50–0.60 to 1.30. Figure 13 shows the solution developed for the Normandie Bridge, which is patented by Freyssinet and re-used in all its later applications. The HPDE ducts are equipped with two imbricated helical filets, about 1.6 mm deep, having a pitch length of 60 cm each.

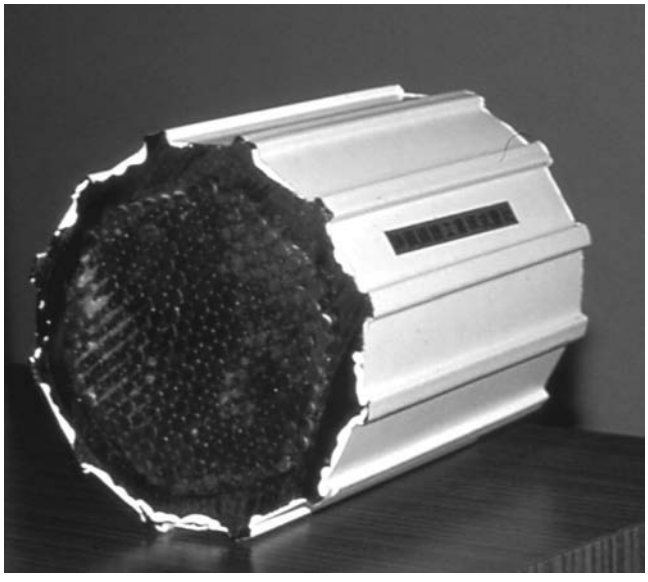

Figure 12. A duct from the Higashi-Kobe Bridge.

Figure 14 gives the results of the first wind tunnel tests, performed by the CSTB at Nantes for the Normandie Bridge. Results have been reported in (Virlogeux 1998a, 1998b) with an error in the legend which is corrected here. The helical filets were 1.3 mm deep in the test, but the bridge has been erected with filets 1.6 mm deep.

Figure 15 gives the results of new wind tunnel tests performed by the CSTB in August 2003. The figure shows

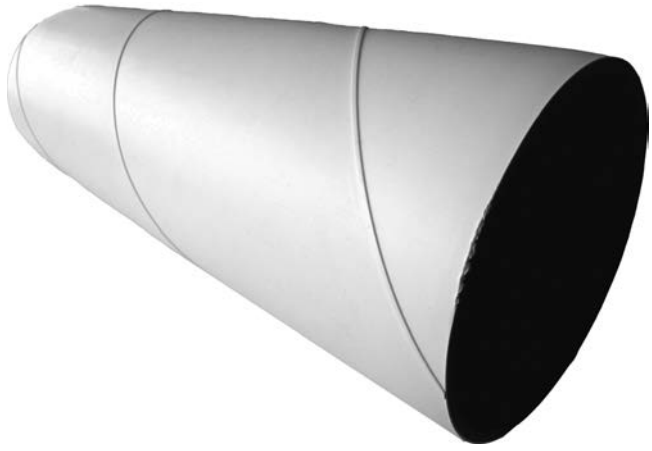

Figure 13. A recent pipe for a Freyssinet stay cable, with two imbricated helical filets.

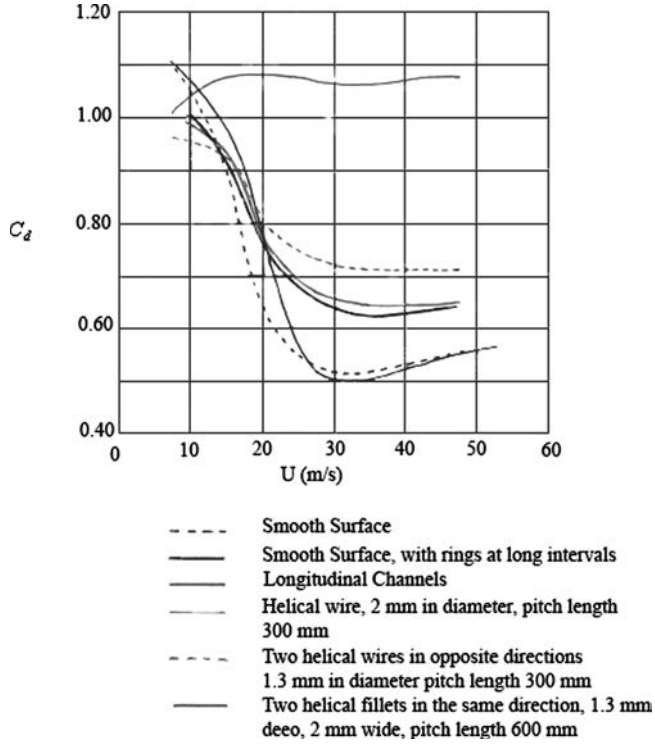

Figure 14. Drag coefficients measured by the CSTB with different profiles for the Normandie Bridge.

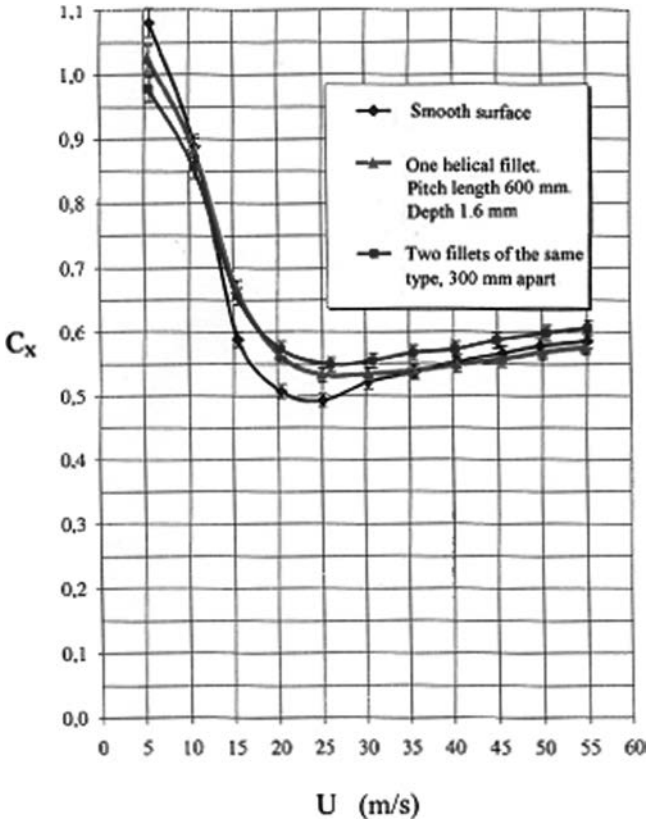

Figure 15. Drag coefficients of three HDPE pipes; a typical cylinder; a cylinder equipped with one helical filet, and a cylinder provided with two helical filets.

the drag coefficients measured on three HDPE pipes, 20 cm in diameter, a classical smooth cylinder without shaping (the drag coefficient drops down to 0.49 in the critical domain); a cylinder equipped with one helical filet (the CSTB has estimated the filet depth to 1.5 mm; whereas it is in fact 1.6 mm deep; the pitch length is equal to 60 cm); and a cylinder corresponding to the typical Freyssinet design with two imbricated helical filets (of the same type). In the latter case, the drag coefficient is more uniform, ever lower in the undercritical domain, varying from 0.57 to 0.61 with a minimum value of 0.55 for Reynolds numbers varying from 272,000 to 736,000.

Figure 16 displays the results of the wind tunnel tests, performed for the Stonecutters Bridge (Kwork and Wong 2004). The smooth duct gives very low results (about 0.35, the figure is not precise enough to give a more accurate value), and the selected duct equipped with dimples gives a value of about 0.65. The results given for helical filets are in disagreement with those obtained by the CSTB the author has seen the tested ducts at Tonji University. The filets were 2 and 4 mm deep instead of 1.5–1.6 mm for the CSTB tests, and with a very different shape. The filets tested for the Stonecutters Bridge are circular; while those provided for

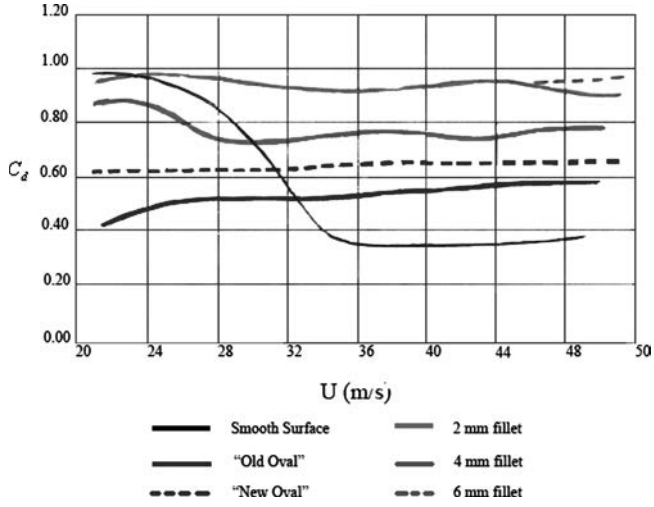

Figure 16. Drag coefficients measured on profiles with dimples (Kwork and Wong 2004).

the Freyssinet ducts have a rectangular shape with rounded upper angles. This large difference in shape might explain the difference in the drag coefficient, between 0.6 and 0.8. Considering the large influence of shapes, even with different distributions of dimples as shown by the Stonecutters tests, it is clear that the tests should be made on the ducts provided by the supplier himself. Additionally, comparative tests should be made in the same laboratory, or by two or three series of tests made in two or three laboratories to eliminate all uncertainties.

4.2 *Wind forces on a stay cable*

In this section, the forces produced, on an inclined stay cable, by a horizontal oblique wind with an average velocity U, are analysed. The inclined stay cable is located in the vertical plane O X Z (figure 17). The cable inclination is noted by α, and the notation β is the angle of azimuth. The unit vectors **I**, **J**, **K** correspond to the three axes, **t** is the unit vector along the cable in the vertical plane, **n** the vector perpendicular to **t** in this plane, **i** the unit vector in the wind direction, and **j** the horizontal unit vector perpendicular to **i**, and the following relationships hold:

$$\mathbf{T} = (\cos\alpha, 0, -\sin\alpha); \quad \mathbf{n} = (\sin\alpha, 0, \cos\alpha);$$
$$\mathbf{i} = (\sin\beta, \cos\beta, 0); \quad \mathbf{j} = (-\cos\beta, \sin\beta, 0)$$

With the classical definition of wind turbulence (figure 18), the wind instantaneous velocity is given by:

$$\mathbf{V} = (U+u)\mathbf{i} + v\,\mathbf{j} + w\mathbf{K} \tag{27}$$

Thus:

$$\mathbf{V} = [(U=u)\sin\beta - v\cos\beta, (U+u)\cos\beta + v\sin\beta, w] \tag{28}$$

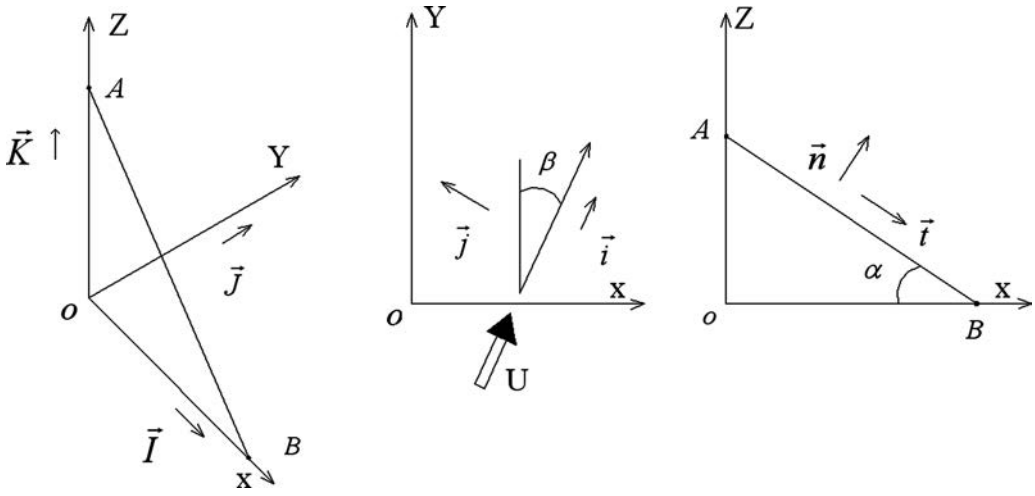

Figure 17. Definition of notations.

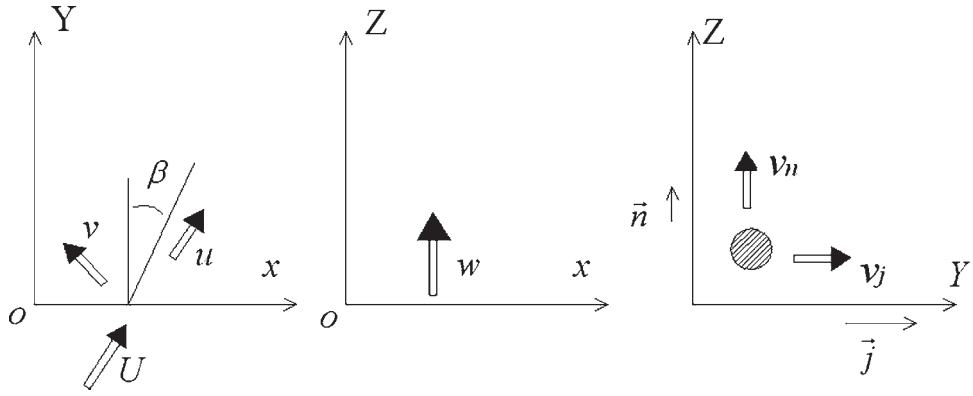

Figure 18. Definition of turbulent wind and cable movement.

This leads to the following result:

$$V^2 = (U+u)^2 + v^2 + w^2 = (U+u)^2$$

Eliminating terms of the second order, one obtains:

$$V = U + u$$

The 'lateral' displacement, along OY and **J**, and the 'vertical' displacement, along **n**, produce a modification of the unit vectors, (**t**,**J**,**n**), which become (**t***,**J***,**n***). For simplification, the vectors (**t***,**J***,**n***) will be assimilated to (**t**,**J**,**n**), considering that the major effects of the cable movements come from the influence of the cable velocity:

$$\mathbf{V}_{\text{cable}} = v_{\text{J}}\mathbf{J} + v_{\text{n}}\mathbf{n}$$

The wind relative velocity can then be written:

$$\mathbf{V}_{\text{R}} = \mathbf{V} - v_{\text{J}}\mathbf{J} - v_{\text{n}}\mathbf{n} \tag{29}$$

In the O X Y Z axes:

$$\mathbf{V}_{\text{R}} = [(U+u)\sin\beta - v\cos\beta - v_{\text{n}}\sin\alpha, (U+u)\cos\beta + v\sin\beta - v_{\text{J}}, w - v_{\text{n}}\cos\alpha] \tag{30}$$

From equation (29), neglecting terms of the second order, one obtains:

$$\mathbf{V}_{\text{R}}^2 = V^2 - 2v_{\text{J}}\mathbf{V}.\mathbf{J} - 2v_{\text{n}}\mathbf{V}.\mathbf{n}$$

Thus:

$$\mathbf{V}_{\text{R}} = U + u - v_{\text{J}}\cos\beta - v_{\text{n}}\sin\alpha\sin\beta \tag{31}$$

The unit vector along $\mathbf{V}_{\text{R}}$, noted as **k**, is given by:

$$\mathbf{k} = \begin{cases} \sin\beta - \left[\dfrac{v}{U} - \dfrac{v_{\text{J}}}{U}\sin\beta + \dfrac{v_{\text{n}}}{U}\sin\alpha\cos\beta\right]\cos\beta \\ \cos\beta + \left[\dfrac{v}{U} - \dfrac{v_{\text{J}}}{U}\sin\beta + \dfrac{v_{\text{n}}}{U}\sin\alpha\cos\beta\right]\sin\beta \\ \dfrac{w}{U} - \dfrac{v_{\text{n}}}{U}\cos\alpha \end{cases} \tag{32}$$

4.3 *A simplified approach for wind forces on a stay cable*

Wind effects are assumed quasi-stationary; that is to say that at any given time, wind forces are the same as those produced by a permanent wind, which has a velocity equal to the instantaneous velocity at that particular time. This is

a reasonable assumption due to the very limited size of the cable compared with the distance crossed by the wind during a time corresponding to the cable vibration period, at least for the main modes.

A traditional and simplified approach consists in assuming that wind forces are given by the projection of the wind relative velocity on the (**J**,**n**) plane which is perpendicular to the cable. The projection of the wind relative velocity on the cable direction is assumed to have no effect.

Since the system (**t***,**J***,**n***) is assimilated to(**t**,**J**,**n**), one can write:

$$\mathbf{V}_{\text{perp}} = (\mathbf{V}_{\text{R}}\mathbf{J})\mathbf{J} + (\mathbf{V}_{\text{R}}\mathbf{n})\mathbf{n}$$

Using equations (26) and (30) renders:

$$\begin{aligned}\mathbf{V}_{\text{perp}} = {} & [(U+u)\cos\beta + v\sin\beta - v_{\text{J}}]\mathbf{J} + [(U+u)\sin\alpha\sin\beta \\ & - v\sin\alpha\cos\beta + w\cos\alpha - v_{\text{n}}]\mathbf{n}\end{aligned} \tag{33}$$

Neglecting terms of the second order, equation (33) gives:

$$\begin{aligned}\mathbf{V}_{\text{perp}}^2 = {} & (U+u)^2(\cos^2\beta + \sin^2\alpha\sin^2\beta) + 2Uv\cos^2\alpha\cos\beta\sin\beta \\ & + 2Uw\cos\alpha\sin\alpha\sin\beta - 2Uv_{\text{J}}\cos\beta - 2Uv_{\text{n}}\sin\alpha\sin\beta\end{aligned}$$

Noting:

$$\begin{aligned}\Delta &= \cos^2\beta + \sin^2\alpha\sin^2\beta \\ &= \sin^2\alpha + \cos^2\alpha\cos^2\beta \\ &= 1 - \cos^2\alpha\sin^2\beta\end{aligned} \tag{34}$$

one obtains:

$$\begin{aligned}V_{\text{perp}} = {} & (U+u)\sqrt{\Delta} + \frac{v\cos^2\alpha\cos\beta\sin\beta}{\sqrt{\Delta}} \\ & + \frac{w\cos\alpha\sin\alpha\sin\beta}{\sqrt{\Delta}} - \frac{v_J\cos\beta}{\sqrt{\Delta}} - \frac{v_n\sin\alpha\sin\beta}{\sqrt{\Delta}}\end{aligned} \tag{35}$$

The average perpendicular velocity can be written (figure 19)

$$\mathbf{U}_{\text{perp}} = U\cos\beta\,\mathbf{J} + U\sin\alpha\sin\beta\,\mathbf{n} \tag{36}$$

with

$$\mathbf{U}_{\text{perp}} = U\sqrt{(\cos^2\beta + \sin^2\alpha\sin^2\beta)} \tag{37}$$

and the angle of incidence of the average perpendicular wind velocity is given from equations (36) and (37) by:

$$\sin i_0 = \frac{\sin\alpha\sin\beta}{\sqrt{\cos^2\beta + \sin^2\alpha\sin^2\beta}} \tag{38}$$

Noting by **r** the unit vector along $\mathbf{U}_{\text{perp}}$ and **q** the perpendicular unit vector, one has the expressions for **r** and **q**:

$$\mathbf{r} = \frac{\cos\beta}{\sqrt{\Delta}}\mathbf{J} + \frac{\sin\alpha\sin\beta}{\sqrt{\Delta}}\mathbf{n}; \quad \mathbf{q} = -\frac{\sin\alpha\sin\beta}{\sqrt{\Delta}}\mathbf{J} + \frac{\cos\beta}{\sqrt{\Delta}}\mathbf{n} \tag{39}$$

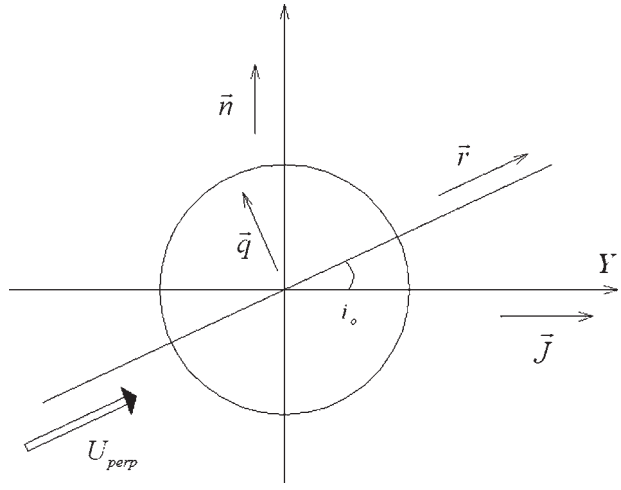

Figure 19. Average perpendicular wind velocity in the (**J**,**n**) plane.

By definition **q** is equal to **tr**. Then, the following product is expressed as:

$$\mathbf{V}_{\text{perp}}.\mathbf{q} = -\frac{v\sin\alpha}{\sqrt{\Delta}} + \frac{w\cos\alpha\cos\beta}{\sqrt{\Delta}} + \frac{v_{\text{J}}\sin\alpha\sin\beta}{\sqrt{\Delta}} - \frac{v_{\text{n}}\cos\beta}{\sqrt{\Delta}}$$

It is concluded that the angle of attack of the relative and instantaneous wind velocity is given by:

$$\begin{aligned}i &= i_0 + \Delta_i \\ &= i_0 + \frac{-v\sin\alpha + w\cos\alpha\cos\beta + v_{\text{J}}\sin\alpha\sin\beta - v_{\text{n}}\cos\beta}{U(\cos^2\beta + \sin^2\alpha\sin^2\beta)}\end{aligned} \tag{40}$$

The unit vector along $\mathbf{V}_{\text{perp}}$ is written as:

$$\begin{aligned}\mathbf{r}^* = {} & \frac{1}{\sqrt{\Delta}}\left[\cos\beta + \left(\frac{v}{U}\sin\alpha - \frac{w}{U}\cos\alpha\cos\beta\right.\right. \\ & \left.\left. - \frac{v_{\text{J}}}{U}\sin\alpha\sin\beta + \frac{v_{\text{n}}}{U}\cos\beta\right)\frac{\sin\alpha\sin\beta}{\Delta}\right]\mathbf{J} \\ & + \frac{1}{\sqrt{\Delta}}\left[\sin\alpha\sin\beta - \left(\frac{v}{U}\sin\alpha - \frac{w}{U}\cos\alpha\cos\beta\right.\right. \\ & \left.\left. - \frac{v_{\text{J}}}{U}\sin\alpha\sin\beta + \frac{v_{\text{n}}}{U}\cos\beta\right)\frac{\cos\beta}{\Delta}\right]\mathbf{n}\end{aligned} \tag{41}$$

The vector perpendicular to **r*** in the (**J**,**n**) plane is equal to **tr***:

$$\begin{aligned}\mathbf{q}^* = {} & \frac{1}{\sqrt{\Delta}}\left[-\sin\alpha\sin\beta + \left(\frac{v}{U}\sin\alpha - \frac{w}{U}\cos\alpha\cos\beta\right.\right. \\ & \left.\left. - \frac{v_{\text{J}}}{U}\sin\alpha\sin\beta + \frac{v_{\text{n}}}{U}\cos\beta\right)\frac{\cos\beta}{\Delta}\right]\mathbf{J} \\ & + \frac{1}{\sqrt{\Delta}}\left[\cos\beta + \left(\frac{v}{U}\sin\alpha - \frac{w}{U}\cos\alpha\cos\beta\right.\right. \\ & \left.\left. - \frac{v_{\text{J}}}{U}\sin\alpha\sin\beta + \frac{v_{\text{n}}}{U}\cos\beta\right)\frac{\sin\alpha\sin\beta}{\Delta}\right]\mathbf{n}\end{aligned} \tag{42}$$

This can also by written as:

$$\begin{cases} \mathbf{r}^* = \mathbf{r} - \left(\dfrac{v}{U}\sin\alpha - \dfrac{w}{U}\cos\alpha\cos\beta \right. \\ \qquad\qquad \left. - \dfrac{v_J}{U}\sin\alpha\sin\beta + \dfrac{v_n}{U}\cos\beta \right) \dfrac{\mathbf{q}}{\Delta} \\ \mathbf{q}^* = \mathbf{q} + \left(\dfrac{v}{U}\sin\alpha - \dfrac{w}{U}\cos\alpha\cos\beta \right. \\ \qquad\qquad \left. - \dfrac{v_J}{U}\sin\alpha\sin\beta + \dfrac{v_n}{U}\cos\beta \right) \dfrac{\mathbf{r}}{\Delta} \end{cases} \tag{43}$$

The cable being a circular cylinder with a diameter D, the expression for wind forces can be written as:

$$F = \frac{1}{2}\rho\, C_d\, D\, V_{perp}\, V_{perp} \tag{44}$$

where C_d is the classical drag coefficient of the cable, and the wind force can be developed as follows:

$$\mathbf{F} = \frac{1}{2}\rho\, C_d\, D \left[\begin{array}{l} (U+u)^2\cos\beta\sqrt{\Delta} \\ \quad + \dfrac{v\,U\sin\beta[\sin^2\alpha + 2\cos^2\alpha\cos^2\beta]}{\sqrt{\Delta}} \\ \quad + \dfrac{w\,U\cos\alpha\sin\alpha\cos\beta\sin\beta}{\sqrt{\Delta}} \\ \quad - \dfrac{v_J\,U[2\cos^2\beta + \sin^2\alpha\sin^2\beta]}{\sqrt{\Delta}} \\ \quad - \dfrac{v_n\,U\sin\alpha\cos\beta\sin\beta}{\sqrt{\Delta}} \end{array} \right] \mathbf{J}$$

$$+ \frac{1}{2}\rho\, C_d\, D \left[\begin{array}{l} (U+u)^2\sin\alpha\sin\beta\sqrt{\Delta} \\ \quad - \dfrac{v\,U\sin\alpha\cos\beta[1 - 2\cos^2\alpha\sin^2\beta]}{\sqrt{\Delta}} \\ \quad + \dfrac{w\,U\cos\alpha[\cos^2\beta + 2\sin^2\alpha\sin^2\beta]}{\sqrt{\Delta}} \\ \quad - \dfrac{v_J U\sin\alpha\cos\beta\sin\beta}{\sqrt{\Delta}} \\ \quad - \dfrac{v_n U[\cos^2\beta + 2\sin^2\alpha\sin^2\beta]}{\sqrt{\Delta}} \end{array} \right] \mathbf{n} \tag{45}$$

The validity of the evaluation can be validated by a classical test which gives the wind forces on a horizontal cylinder ($\alpha = 0$) in the (**i**, **j**) axes, through the ratios:

$$\frac{F_i}{\frac{1}{2}\rho U^2 C_d\, D} \quad \text{and} \quad \frac{F_j}{\frac{1}{2}\rho U^2 C_d\, D}$$

For a uniform wind ($v = w = v_j = v_n = 0$); and for a horizontal stay cable ($\alpha = 0$), equation (45) is reduced to:

$$\mathbf{F} = 1/2\,\rho\, U^2 C_d\, D\cos^2\beta$$
$$\mathbf{J} = 1/2\,\rho\, U^2\, C_d\, D[\cos^3\beta\ \mathbf{i} + \cos^2\beta\sin\beta\ \mathbf{j}]$$

Figure 20 demonstrates the excellent agreement of the approximation.

4.4 *An alternative approach for wind forces on a stay cable*

The cable, a circular cylinder, is symmetrical with respect to any plane containing the vector, **t**, and the wind flow is governed by the vector **i** for the average wind velocity, or **k**, for the instantaneous wind velocity. It is then clear that the wind flow around the cable is symmetrical with respect to the plane containing the vectors, **i** (**k**) and **t**. Assuming, as a first approximation, that the flow is bidimensional, one can analyse the wind profile in any plane containing the vector **i** (**k**) and the unit vector perpendicular to the plane containing **i** (**k**) and **t**. If the analysis is limited to the average wind, this unit vector is the vector **q** already given earlier as **tr**. One can write that:

$$\mathbf{i} = \mathrm{A}\mathbf{t} + \mathrm{B}\mathbf{r}$$

Thus:

$$\frac{\mathbf{t}\wedge\mathbf{i}}{|\mathbf{t}\wedge\mathbf{i}|} = \frac{\mathbf{t}\wedge(\mathrm{A}\mathbf{t} + \mathrm{B}\mathbf{r})}{|\mathbf{t}\wedge(\mathrm{A}\mathbf{t} + \mathrm{B}\mathbf{r})|} = \mathbf{t}\wedge\mathbf{r}$$

The angle φ between the cable axis, **t**, and the wind velocity, **i**, is given by (figure 21):

$$\cos\varphi = \mathbf{t}\,\mathbf{i} = \cos\alpha\sin\beta \tag{46}$$

The cable apparent profile in the wind, in the plane (**i**, **q**), is elliptical with a short diameter D and a long diameter E, as shown in figure 22:

$$E = \frac{D}{\sin\varphi} = \frac{D}{\sqrt{\cos^2\beta + \sin^2\alpha\sin^2\beta}} \tag{47}$$

The angle of attack is equal to zero:

$$i = 0 \tag{48}$$

The same result is obtained with the relative wind velocity by the definition of the unit vector **q***, perpendicular to **t** and **k**, which is mentioned earlier, as **tr***.

The angle, φ*, between the cable axis, **t**, and the wind relative velocity, **k**, is given by:

$$\cos\varphi^* = \mathbf{t}.k = \sin\beta - \left[\frac{v}{U} - \frac{v_J}{U}\sin\beta + \frac{v_n}{U}\sin\alpha\cos\beta\right]\cos\beta \tag{49}$$

Finally, one obtains the same result, the apparent angle of attack is at any time equal to zero, regardless of the variations of the components of wind turbulence and cable movements. The apparent profile constantly changes with these variations and movement; it is elliptical with a short diameter still equal to D and a long diameter, E^*, given by:

$$\mathbf{E}^* = \frac{D}{\sin\varphi^*} = \frac{D}{\sqrt{1 - \cos^2\varphi^*}} \tag{50}$$

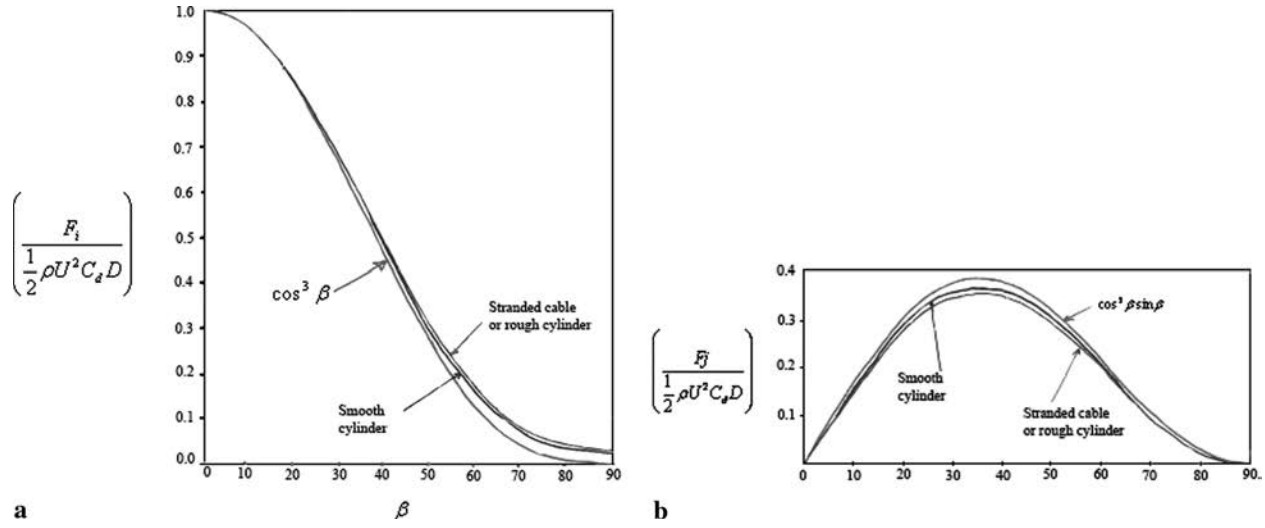

Figure 20. Classical test for oblique winds.

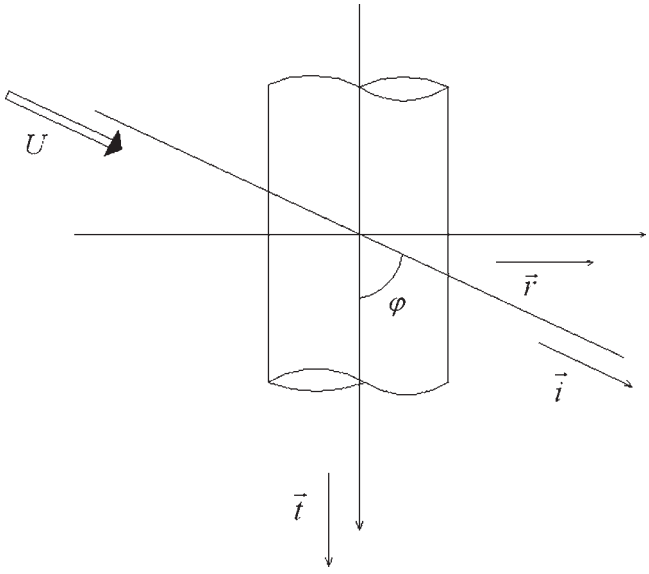

Figure 21. Definition of the angle φ.

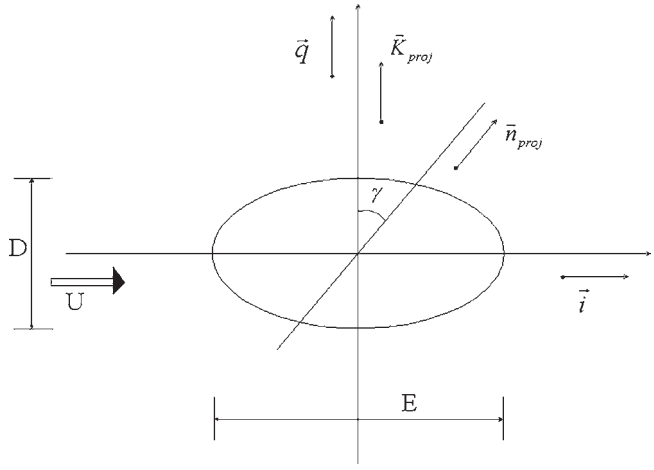

Figure 22. Wind velocity in the plane (**i**,**q**).

It is important to locate the projections of the vectors **k** and **n** in the plane (**i**,**q**). Since **ik** is equal to zero, the projection of **k** is along **q**, which appears as 'vertical', and one can write:

$$\mathbf{k}.\mathbf{q} = \frac{\cos\alpha\cos\beta}{\sqrt{\cos^2\beta + \sin^2\alpha\sin^2\beta}} \tag{51}$$

As for **n**, the following expression is written:

$$\mathbf{n}.\mathbf{i} = \sin\alpha\sin\beta; \quad \mathbf{n}.\mathbf{q} = \frac{\cos\beta}{\sqrt{\cos^2\beta + \sin^2\alpha\sin^2\beta}}$$

The projection of **n** can be given by the angle γ with the vector **q**:

$$\mathrm{tg}\gamma = \frac{\sin\alpha\sin\beta}{\cos\beta}\sqrt{\cos^2\beta + \sin^2\alpha\sin^2\beta} \tag{52}$$

A tentative evaluation of wind forces through a drag coefficient corresponding to the apparent elliptical profile would be misleading since the drag force is not in the wind direction, but perpendicular to the stay-cable axis, **t**. The drag forces correspond to the integration of pressure forces on the stay cable surface, which are individually perpendicular to the stay cable axis when viscosity is neglected.

It is worth noting that, in fact, the wind flow is not bidimensionnal. There is a deviation of the flow along the cable axis. However, this result does not change the fact that the flow is symmetrical with respect to the (**t**,**k**) plane;

even with a deviation along **t**, the angle of attack is equal to zero as well as the lift force.

5. Damping of stay cables

5.1 *Internal damping*

The internal damping of stay cables depends, greatly, on the cable technology. All the values given below are ratio to critical. The logarithmic decrement is obtained by multiplying these values by $2\pi/1-\xi$.

In the Saint-Nazaire Bridge, which has locked coil cables with a hardening product between the wires, the damping coefficient is 0.1%. In the Brotonne Bridge, with cables made of parallel strands injected with cement grout in a steel pipe, the damping coefficient is 0.01%. In the Seyssel Bridge, with locked coil cables with amorphous polyethylene between wires, the damping coefficient is 0.05%. In the Second Severn crossing, with parallel auto-protected strands in external polyethylene duct, the damping coefficient ranged from 0.1 to 0.6% according to test results, which are surprisingly high. In the Vasco de Gama Bridge, in Lisbon, also with parallel auto-protected strands in external polyethylene duct, the measured damping coefficient is about 0.13%. In the Erasmus Bridge, with parallel auto-protected strands in external polyethylene duct, the damping coefficient has been estimated as 0.2%. Finally, in the Iroise Bridge over the Elorn River, with cables made of parallel galvanised strands injected with oil wax in a polyethylene duct, the damping coefficient is 0.14%.

The following damping values are considered:

- Injection with cement grout: 0.01%.
- Locked coil cables: 0.1%.
- Parallel individually protected strands: 0.1–0.15%.
- Parallel strands injected with oil wax: 0.15%.

It should be noted that measures have to be made when there is no wind, to eliminate aerodynamic damping.

5.2 *Aerodynamic damping for transverse winds*

Starting with a simple approach, assume that the wind is perpendicular to the bridge. In other words, perpendicular to the plane O X Z, that is for an azimuth angle, β, equal to zero (figure 23). When the cable moves in the wind direction with a velocity, v_{J}, the relative velocity is $(U-v_{\mathrm{J}})$ and the wind force is given by:

$$F=\frac{1}{2}\,\rho(U-v_{\mathrm{J}})^2 DC_{\mathrm{d}}=\frac{1}{2}\,\rho U^2 DC_{\mathrm{d}}-\rho UDC_{\mathrm{d}}v_{\mathrm{J}}$$

whereas the damping force is expressed by:

$$f(x,t)=-\rho\,U\,D\,C_{\mathrm{d}}v_{\mathrm{J}}(x,t)$$

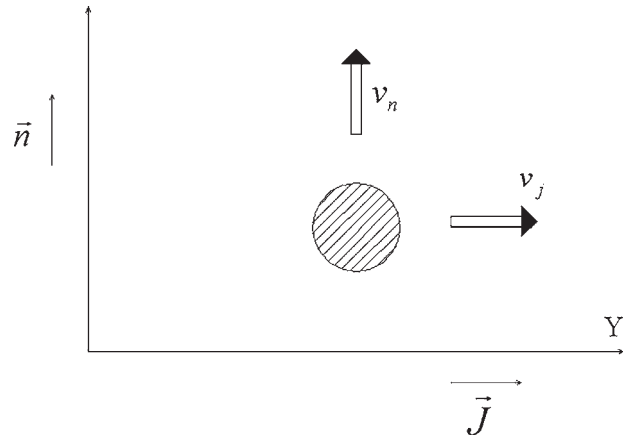

Figure 23. Wind perpendicular to the bridge.

As shown earlier:

$$y(x,t)=\sum_{i=1}^{n}\sin\left(\frac{i\pi x}{L}\right)y_i(t)$$

thus:

$$v_{\mathrm{J}}(x,t)=\sum_{i=1}^{n}\sin\left(\frac{i\pi x}{L}\right)y_i(t)$$

From equation (14), the generalised damping force corresponding to mode k, can be evaluated as:

$$\begin{aligned}f_k(t)&=-\frac{2}{mL}\int_0^L\rho UDC_{\mathrm{d}}\left[\sin\left(\frac{k\pi x}{L}\right)\right]^2\mathrm{d}x\,y_k'(t)\\&=-\frac{\rho UDC_{\mathrm{d}}}{m}y_k'(t)\end{aligned}$$

Referring to equation (15), the damping coefficient in mode k (ratio to critical) for 'lateral' vibrations is given by:

$$\xi_k=\frac{\rho UD\,C_{\mathrm{d}}}{2m\omega_k}\tag{53}$$

where ω_k is the pulsation of the stay cable in mode k.

When the cable moves 'vertically', that is in the vertical plane O X Z, with a velocity v_{n}, the apparent angle of incidence is $(-v_{\mathrm{n}}/U)$, and the wind force is given by:

$$F_n=\frac{1}{2}\rho U^2 D\,C_\ell(\mathrm{i})=\frac{1}{2}\rho U^2 D\frac{\mathrm{d}C_\ell}{di}(o)i$$

Finally:

$$F_n=-\frac{1}{2}\rho U^2 D\,C_{\mathrm{d}}\frac{\mathrm{v_n}}{\mathrm{U}}=-\frac{1}{2}\rho UDC_{\mathrm{d}}\mathrm{v_n}$$

The damping force is written as:

$$f(x,t)=-1/2\,\rho U\,D\,C_{\mathrm{d}}v_{\mathrm{n}}(x,t)$$

As shown above, the generalised damping force corresponding to mode k is evaluated as:

$$f_k(t) = -\frac{2}{mL}\int_0^L \left[\frac{1}{2}\rho U D C_d\right]\left[\sin\left(\frac{k\pi x}{L}\right)\right]^2 dx\, y'_k(t)$$
$$= -\frac{\rho U D\, C_d}{2m} y'_k t(x)$$

Thus the damping coefficient in mode k (ratio to critical) for 'vertical' vibrations:

$$\xi_k = \frac{\rho U D\, C_d}{4m\omega_k} \tag{54}$$

The damping coefficient given by equation (54) is only half of the value that results from equation (53). This explains, at least partly, the fact that cables are generally more prone to 'vertical' than to transverse vibrations.

5.3 *Aerodynamic damping for oblique winds*

From the results of section 4.3, the aerodynamic damping coefficients in oblique winds can be evaluated. From equation (45), the damping force corresponding to 'lateral' cable vibrations is equal to:

$$\mathbf{F}(x,t) = -\frac{1}{2}\rho C_d D U\left(\frac{2\cos^2\beta + \sin^2\alpha\sin^2\beta}{\cos^2\beta + \sin^2\alpha\sin^2\beta}\right) v_J(x,t)\mathbf{J}$$

Following the same principles as in section 5.2, the damping coefficient that corresponds to mode k as a ratio to critical is given by:

$$\xi = \frac{\rho U D\, C_d}{4m\omega_k}\left(\frac{2\cos^2\beta + \sin^2\alpha\sin^2\beta}{\cos^2\beta + \sin^2\alpha\sin^2\beta}\right) \tag{55}$$

For vertical vibrations, one obtains:

$$\mathbf{F}(x,t) = -\frac{1}{2}\rho C_d D U\left(\frac{\cos^2\beta + 2\sin^2\alpha\sin^2\beta}{\cos^2\beta + \sin^2\alpha\sin^2\beta}\right) v_n(x,t)\mathbf{n}$$

This force corresponds for mode k to a damping coefficient:

$$\xi = \frac{\rho U D\, C_d}{4m\omega_k}\left(\frac{\cos^2\beta + 2\sin^2\alpha\sin^2\beta}{\cos^2\beta + \sin^2\alpha\sin^2\beta}\right) \tag{56}$$

When the azimuth angle, β, is equal to zero, equations (55) and (56) are reduced to equations (53) and (54).

6. Cable vibrations

Many factors and phenomena can produce cable vibrations, therefore a careful and extensive analysis is needed. At the same time it is necessary to classify the different causes of cable vibrations as demonstrated in the following.

6.1 *Vortex shedding*

A smooth flow passing around a given profile produces vortices, alternatively on the upper and lower sides, and induces forces perpendicular to the wind direction. Wind turbulence normally reduces the intensity of vortex shedding. The frequency of the exciting force is given by:

$$N = \frac{US}{H} \tag{57}$$

where U is the wind velocity in m s^{-1}, H is the profile depth in metres, D is the cable diameter, and S is the Strouhal number which is about 0.18 for a circular cylinder. Vortex shedding can excite a cable in mode k, whose period is T_k, when the wind velocity has a critical value of:

$$U_c = \frac{D}{0.18T_k} \tag{58}$$

The so-called cable-galloping which appears, according to new theories, to be a specific type of vortex shedding will be evoked later in this paper. As shown by Matsumoto *et al.* (1999), axial vortices flow along the stay cable, enhance every third classical Von Karman vortex, in oblique winds. This produces an increased excitation, perpendicular to the wind flow, with a frequency equal to one-third of the classical shedding frequency:

$$N = \frac{US}{3D} \tag{59}$$

The Strouhal number is reduced to about 0.15 in these situations, leading to a critical velocity of:

$$U_c = \frac{3D}{0.15T_k} \tag{60}$$

to produce an excitation on mode k.

Due to the very small diameter of stay cables, the critical velocities corresponding to classical vortex shedding, as given by equation (58), are very low, and associated with very low wind energy. The only example of significant cable vibrations due to direct and classical vortex shedding to the author's knowledge took place at the Saint-Nazaire Bridge.

One stay cable suffered from high frequency vibrations, in modes 25 to 45. It is worth noting that the same cable was a replacement for an existing stay cable which had shown some signs of fatigue and later broke (figure 4). The cable accelerations and the wind velocity were recorded and analysed by Virlogeux and Arcadis. A good correlation between the wind velocity, which varies with turbulence and altitude along the stay cable, and the frequency of the extreme response was demonstrated (figure 24). It should be noted, however, that not all frequencies could appear due to the position of accelerometers.

6.2 *Wake effects*

There are many different types of wake effects. The cables of a cable-stayed bridge can be in the wake of a structural element, or of construction equipment. The classical condition is for bridges with two planes of cables under oblique winds. Some downstream cables are in the wake of the upstream leg of the pylons; especially with H-shaped pylons. The wind flow is disturbed by these pylon legs, which increases the turbulence with very specific distributions of excitations that can produce vibrations in downstream cables (figure 25). The critical velocity is evidently given by the Strouhal formula corresponding to the production of vortices around the waking element:

$$U_c = \frac{H}{ST_k} \tag{61}$$

where H is the transverse dimension of the element, S its Strouhal number, and T_k is the period of the cable excited in mode k.

Through private communications with Jorg Schlaich, the author learned that such specific vibrations have been observed at the Evripos Bridge in Greece. It is also worthy of note that some short stay cables at the Normandie Bridge vibrated once during construction in the wake of a pylon leg. The author considers this information, although not scientifically recorded, credible even if the shape of the pylons, an inverted Y, may limit such effects.

Another condition may be induced with the wake of the whole cable system, when the wind is almost parallel to the bridge. The upwind cables could disturb the flow and produce an excitation of downwind cables. However, due to the frequency of vortex shedding on cables, the author is of the opinion that such vibrations may not develop for large wind velocities.

A more complex phenomenon is produced in twin cables as frequently used in Japan to limit the cable size. Cables are arranged in pairs of parallel cables at close distance, usually few diameters apart, anchored at the same level in the tower and deck. The second cable, shown in figure 26, is in the wake of the first one and then excited by the vortices produced on the first cable. According to previous results, this is not critical. However, a specific interaction develops between the two cables; where the existence of the first cable disturbs the flow around the second, and the movements of the second cable alter the flow around the

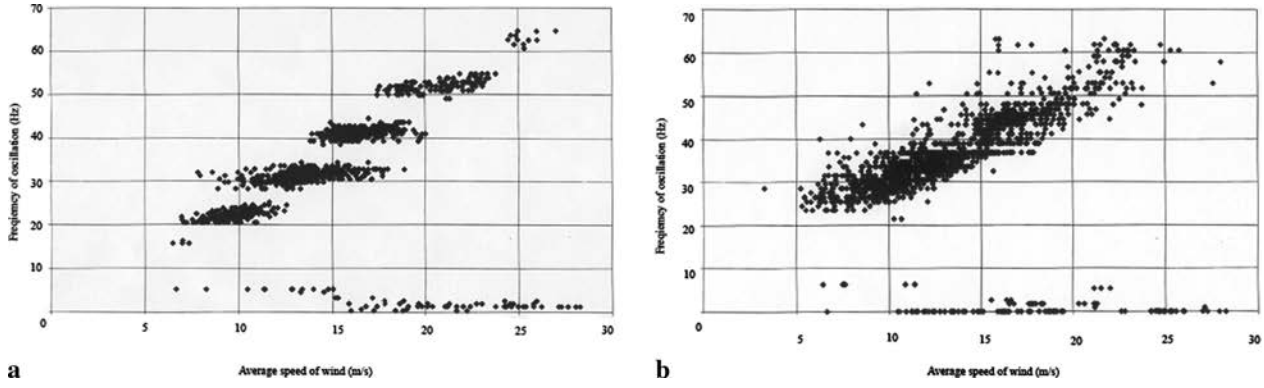

Figure 24. Saint-Nazaire Bridge's stay cables 19 and 32 downstream. Correlation between frequency and wind velocity at deck level (Virlogeux and Arcadis).

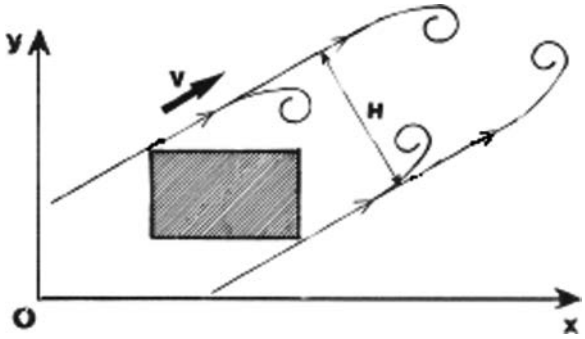

Figure 25. Wake of a pylon leg.

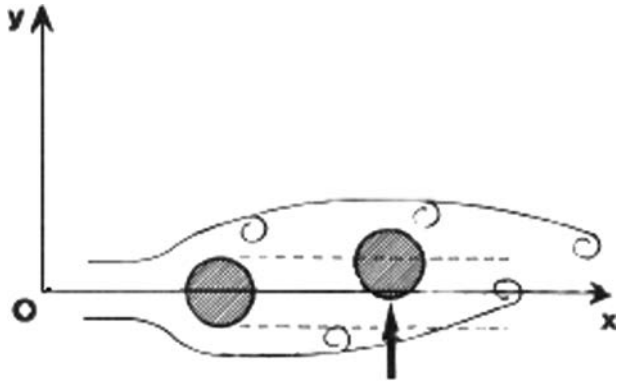

Figure 26. Wake effect in twin cables.

first. This phenomenon decreases, and disappears when the distance between the two cables increases or when they are not exactly parallel.

The same phenomenon develops with much more complex aspects when several cables are grouped; for example, to constitute a strong backstay. This is why the author recommended connecting the numerous cables forming the backstays of the Erasmus Bridge when his opinion was sought regarding the design of the bridge (figure 27).

It is worth noting that a specific problem of the same type exists when cables are made of a bunch of parallel individually protected strands, a technique developed by Freyssinet. Due to aerodynamic interaction between strands, external strands can move outwards and then inwards, shocking the central strands; and finally producing some limited global vibration of the cable. This movement, which is called breathing of strands, and the resulting shocks, produce an important and disagreeable rattling noise. These vibrations have been one of the main reasons to encase individually protected strands in an external duct.

6.3 *Buffeting*

Buffeting has a direct effect on cables as on any flexible structure. These effects grow with the wind velocity, a bit higher than the square of the wind velocity. The buffeting effects, however, do not appear dangerous except if buffeting can produce shocks in aiguilles (or cross cables), if any and when they have received low tensions. Except in this last case, it seems logical that cables are moved by high winds. The effect is not as critical as with other phenomena which are more related to instability, with large vibrations for low or medium winds. Aerodynamic damping on cables helps limiting vibrations, as well as high tensions under permanent loads. It should be noted that buffeting can produce aerodynamic instability in bridges with two parallel planes of stay cables (Davenport 1994). A gust striking the upwind plane of stays will strike the downwind stays at a time B/U later, where B is the distance between the two planes of cables. If the difference corresponds to half a cycle of torsional movement of the deck, whose period is T_t, instability can take place. The critical velocity is then given by:

$$U_c = \frac{2B}{T_t} \tag{62}$$

Figure 27. Six backstays at the Erasmus Bridge attached to avoid wake effects.

6.4 *Aerodynamic stability*

Different types of aerodynamic instability can develop. When cables do not have the 'perfect' shape of a circular cylinder, their shape may produce some cable galloping. It was shown earlier that drag forces can be very high for long spans. To reduce drag forces on cables, some engineers proposed to group the individually protected strands of the Normandie Bridge in a flat hexagonal arrangement (figures 28 and 29).

However, this would have produced high lift forces in oblique winds and possible galloping effects. In addition, it appeared that the irregular shapes produced by the different strands increase drag forces to very high values. Therefore the author recommended the installation of strands in circular ducts (figure 30).

Cable-strand effects in locked coil cables and even more in large strands with no external duct can produce specific vibrations. Evidently, the pitch length has a significant influence, since the installation of small helical filets on cable ducts can be used to eliminate cable vibrations and thus have exactly the opposite effect. Such effects may explain the high frequency vibrations in the Saint-Nazaire Bridge, but this has not been proved to date. The reasons for these very specific vibrations are still unclear. Ice on cables may be dangerous also, as on electric lines, since ice may change the shape of cables and produce instablility. This is why all elements which can retain water on cables must be eliminated in cold climates. As recent as December 2003 and January 2004, major vibrations at the Oresund Bridge were related to this phenomenon. This is believed to be the case, but the vibrations mainly affected two stay cables (numbers 8 and 10) and not all the longer ones as would be expected logically. In addition, towers are transversally flexible, and may contribute to a parametric excitation of some stay cables.

As mentioned earlier, in studying cable vibrations, the so-called cable-galloping in oblique winds has to be evoked. Stay cables appear elliptical in oblique winds as shown earlier, but this cannot produce any aerodynamic instability, since the angle of attack is always equal to zero. Equation (45) and section 4.4 clearly indicate that there is no unstable factor in the aerodynamic force. It has been

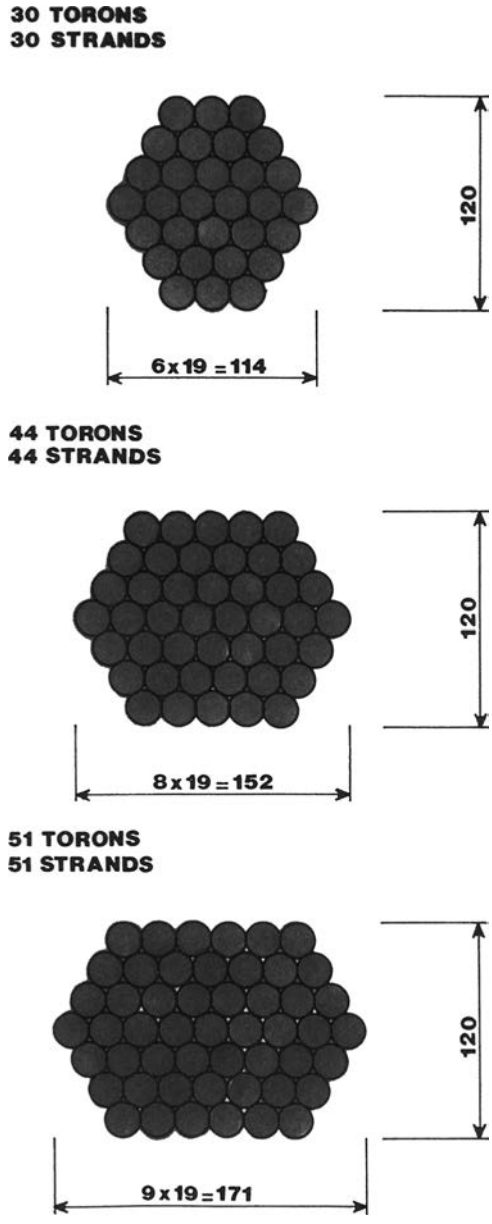

Figure 28. Flat arrangement of stay cables proposed by Freyssinet for the Normandie Bridge.

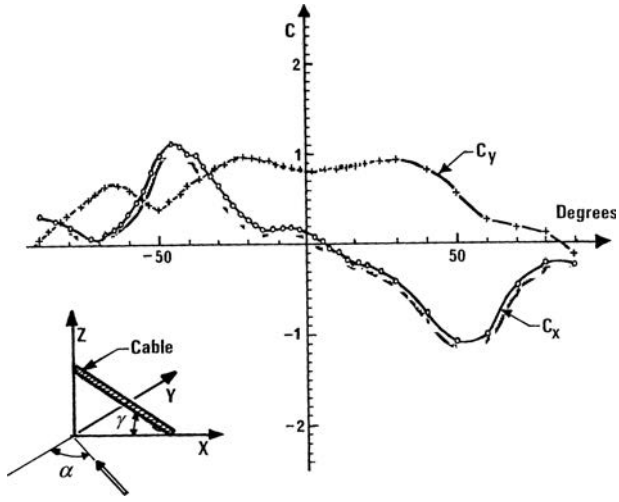

Figure 29. Aerodynamic stationary coefficients of the flat arrangement proposed by Freyssinet, for the Normandie Bridge, as functions of the angle of attack.

shown, however, that when the wind is oblique, with an azimuth angle, β, different from zero, inclined stay cables can suffer from vibrations which have the characteristics of aerodynamic instability, or vertical galloping (Saito *et al.* 1994). This galloping is influenced by the Strouhal number, S_c, given by:

$$S_c = \frac{2m\xi}{\rho D^2} \tag{63}$$

where ρ is the volumetric mass of air, ξ is the damping coefficient in the cable (ratio to critical), m is the lineic mass of the stay cable and D is the cable diameter. Japanese researchers, who have been followed by the PTI Recommendations in the United States (PTI 2001), consider that there is no risk of galloping in oblique winds on mode k when the wind velocity is below a critical value, which is given by:

$$U_c = \frac{CD}{T_k}\sqrt{\frac{S_c}{2}} \tag{64}$$

where C is a constant equal to 40 and T_k is the stay cable vibration period at mode k.

The author does not consider this formula as a criterion. According to equation (64), almost all stay cables would be prone to galloping, if S_c and T_k are replaced by their expressions, equations (63) and (13), which results in:

$$U_c = CD\frac{k}{2L}\sqrt{\frac{F}{m}}\sqrt{\frac{m\xi}{\rho D^2}} = \frac{kC}{2L}\sqrt{\frac{F\xi}{\rho}}$$

In the above formula, neither the lineic mass nor the cable diameter influences the critical velocity.

For a stay cable made of parallel 7 wire strands, the tension under permanent loads can be evaluated by:

$$F = nA\gamma\sigma_{GUTS}$$

where n is the number of strands, A is the area of the strand section (m^2), σ_{GUTS} is the guaranteed ultimate tensile stress (for example 1770 MPa) and γ is a coefficient corresponding to the level of permanent stress in the cable, which normally varies between 0.30 and 0.40 according to the bridge type. Thus the critical velocity can be written as:

$$U_c = \left(\frac{C}{2}\sqrt{\frac{A\sigma_{GUTS}}{\rho}}\right)\frac{k}{L}\sqrt{n\gamma\xi}$$

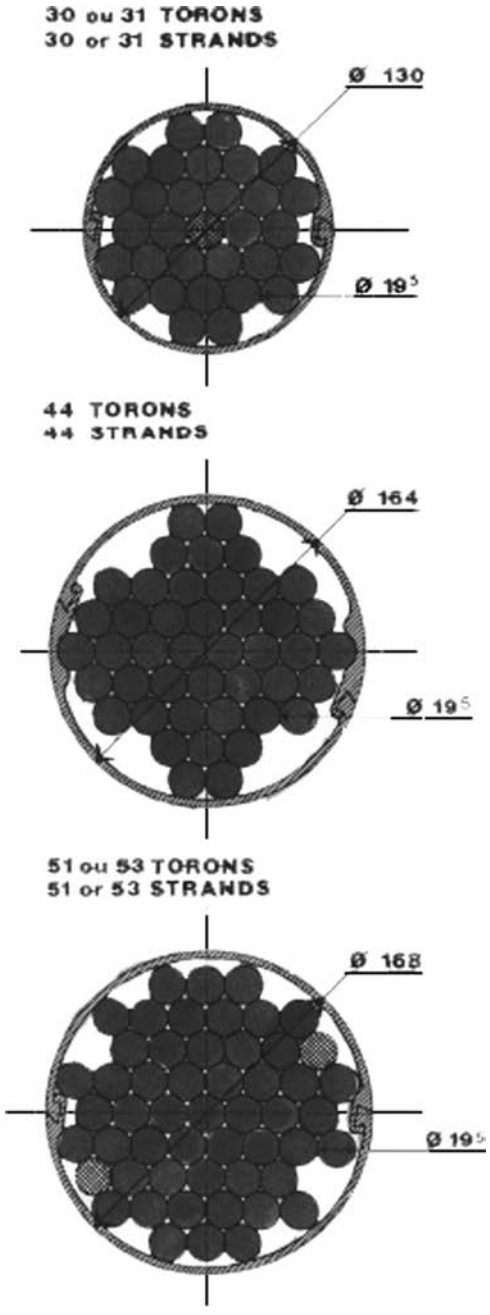

Figure 30. Normandie Bridge's final arrangement of stay cables.

when C is taken equal to 40, $A = 150\,\text{mm}^2$ and $\sigma_{\text{GUTS}} = 1770$ MPa:

$$U_c = 9292\frac{k}{L}\sqrt{n\gamma\xi}$$

As γ varies between 0.30 and 0.40, one obtains:

$$5089\frac{k}{L}\sqrt{n\xi} \le U_c \le 5877\frac{k}{L}\sqrt{n\xi}$$

To give an approximation, one can write:

$$U_c \cong 5500\frac{k}{L}\sqrt{n\xi} \tag{65}$$

For the first mode, the most critical, figure 30 gives the corresponding estimates of the critical velocity as a function of the three main parameters, the cable length, L, the number of strands, n, and the damping coefficient (ratio to critical), ξ. The damping coefficient, ξ, has been assumed at three values. The value of $\xi = 0.1\%$ corresponds to the lowest value for modern cables made of parallel strands, without any damping devices. The level of damping of $\xi = 0.5\%$, which corresponds to the damping level considered acceptable to eliminate rain/wind induced vibrations, is adopted by most designers, including the author. Finally, the value of $\xi = 1\%$ is demonstrated to show that doubling the damping is not efficient. The cable length, L, varies from 50 to 250 m to cover the classical range of cable-stayed bridges. The number of strands, n, corresponds to classical anchorages: 12, 19, 27, 37, 61, and 91.

The above demonstration clearly shows that almost all stay cables would appear unstable according to the proposed criterion, and that even doubling the damping ratio is inefficient.

In the paper by Saito *et al.* (1994), cable vibrations were attributed to the axial flow along the cable. This is more likely as most of the tests recorded in the paper correspond to a wind in the plane of cables, $\beta = 90^\circ$ with the notation adopted in this paper. In addition, only two results (with a star) correspond to a Scruton number higher than 25. It should be noted that the definition cited in Matsumoto *et al.* (1994) uses, $m\delta/\rho D^2$ for the Scruton number, which is slightly different from the definition used in this paper; namely, $2m\delta/\rho D^2$.

In a more recent paper, Matsumoto *et al.* (1999) develop the following convincing theory. When the cable is perpendicular to the wind ($\beta = 0$), the wind flow produces vortex shedding in agreement with the Von Karman formula, given by equation (57) of this paper:

$$N = \frac{US}{D}$$

where N is the shedding frequency, in Hz, S is the Strouhal number, U the wind velocity, and D the cable diameter. The Strouhal number for a circular cylinder is equal to 0.18. When the wind is oblique to the cable, the Strouhal number decreases and becomes equal to 0.15 (for $\beta > 20$ or 30°). Axial vortices flow along the stay cable in oblique winds, enhancing every third classical Von Karman vortex. This phenomenon produces an increased excitation, perpendicular to the wind flow, with a frequency equal to one-third of the classical shedding frequency:

$$Nc = \frac{US}{3D} \tag{66}$$

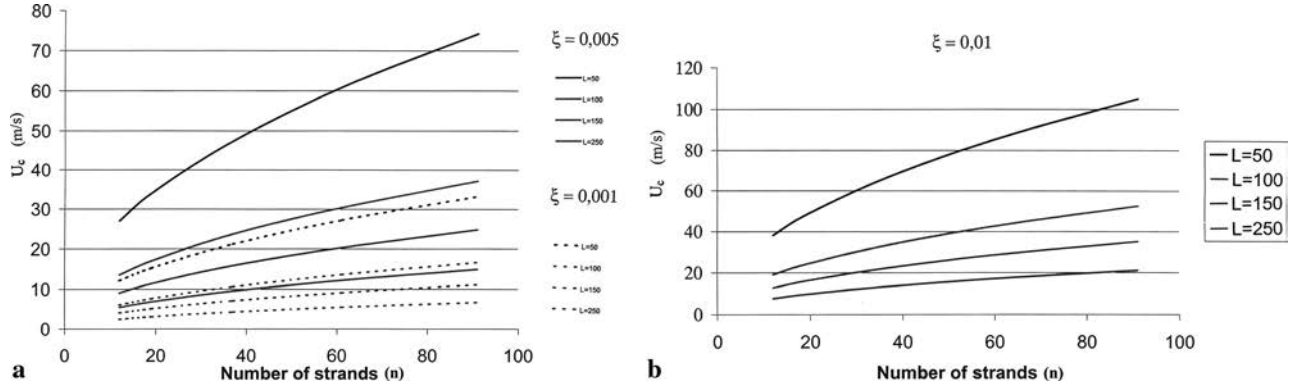

Figure 31. Critical wind velocity, from the criterion proposed for galloping, as a function of the three parmeters, L, n, and ξ.

and for multiple periods:

$$N_i = \frac{US}{3iD} \quad \text{for } i = 1, 2 \ldots n \tag{67}$$

The corresponding reduced velocities are given by:

$$U_{\mathrm{R}ci} = \frac{U}{N_i} = \frac{3i}{S}$$

Replacing S by 0.15 shows that U_{Rci} takes the successive values 20, 40, 60, 80, ... , as shown by Matsumoto *et al.* (1999). This result is satisfactory, since it is believed that the energy produced by this enhanced vortex shedding is limited, so that vibrations might be controlled by some increased damping, in contradiction with equation (64).

It has come to the author's knowledge, during the writing of this paper, that the U.S. Federal Highway Administration (FHWA) sponsored a study devoted to this problem (FHWA Report No. RI98-034 RDT05-004, 2005). The study was conducted by a team led by HNTB Corporation, which concluded that dry cable-galloping cannot occur unless the level of damping is very low. This confirms the author's opinion, which is more based on practical experience.

The last type of aerodynamic instability is directly produced by the drop in the drag coefficient of circular cylinders when the Reynolds number reaches the critical value. Limiting the analysis to perpendicular winds, it is supposed that the cable vibrates in the wind direction with a velocity of $v_{\mathrm{J}}(t)$; the relative velocity is then (figure 23):

$$V_{\mathrm{r}} = U - v_{\mathrm{J}}(t)$$

The drag force can be written as:

$$\mathrm{F} = \frac{1}{2}\rho D(U - v_{\mathrm{J}})^2 C_{\mathrm{d}}(U - v_{\mathrm{J}})$$

The first order is then developed as follows:

$$F = \frac{1}{2}\rho D U^2 C_{\mathrm{d}}(U) - \frac{1}{2}\rho D U^2 \left[2C_{\mathrm{d}}(U) + U\frac{\mathrm{d}C_{\mathrm{d}}}{\mathrm{d}U}(U)\right]\frac{v_{\mathrm{J}}}{U}$$

The second factor is a damping factor, except when the derivative of the drag coefficient becomes negative:

$$\frac{\mathrm{d}C_{\mathrm{d}}}{\mathrm{d}U} < -\frac{2C_{\mathrm{d}}(U)}{U} \tag{68}$$

Then aerodynamic forces tend to accelerate vibration and may produce the 'drag crisis'.

Referring to section 5.2, one can evaluate the damping coefficient for transverse vibrations in mode k (ratio to critical) by:

$$\xi_k = \frac{\rho UD}{2m\omega_k}\left[C_{\mathrm{d}}(U) + \frac{U}{2}\frac{\mathrm{d}C_{\mathrm{d}}}{\mathrm{d}U}(u)\right] \tag{69}$$

A drag crisis will take place when the total damping coefficient, including the stay cable internal damping, becomes negative:

$$\xi_t = \xi + \frac{\rho UD}{2m\omega_k}\left[C_{\mathrm{d}}(u) + \frac{U}{2}\frac{\mathrm{d}C_{\mathrm{d}}}{\mathrm{d}U}(u)\right] < 0 \tag{70}$$

The author has never observed such a possibility for tested cable ducts, but the following is worthy to note. In any case, for Reynolds numbers in the critical, range of 100,000 – 200,000, that is for wind velocities between 12 and 18 m s^{-1}, the drop in drag coefficients produces a strong reduction of aerodynamic damping of stay cables and favour cable vibrations. Most probably introducing some relief on cable ducts limits the drop of the drag coefficient, as this is the case with the Freyssinet ducts which have been tested by the CSTB. This also contributes to limiting cable vibrations, even when there is no rain as was observed during the erection of the Normandie Bridge.

6.5 *Parametric excitation*

Vibrations of stay cables may be induced by the movements of their anchorages, either on the deck or in the towers. Stay cable vibration could also occur due to the structural

vibrations of deck and towers which can be produced by vortex shedding on deck or tower, buffeting or traffic. The analysis of a cable excited at one of its two ends must be divided into two different categories for better understanding. This is also essential in separating the transverse excitation, perpendicular to the cable direction, from the longitudinal excitation, in the direction of the cable. Extensive theories have been developed to describe the above behaviour. In the following, only straight and horizontal cables will be considered for simplicity.

Considering transverse vibrations produced by the transverse movement at anchorage B:

$$y_{\mathrm{B}}(t) = \mathrm{A}\sin\omega t$$

one can write that the displacement of the typical point, $Y(x,t)$, as the sum of the solid movement produced by the moving anchorage, $y_0(x,t)$, and the relative movements, $y(x,t)$ (figure 32), where $y_0(x,t)$ is given by:

$$y_0(x,t) = \frac{x}{L}A\sin\omega t$$

Considering the cable tension constant, the local dynamic equilibrium of the cable gives:

$$F\frac{\mathrm{d}^2y(x,t)}{\mathrm{d}x^2} = m\frac{\mathrm{d}^2Y(x,t)}{\mathrm{d}t^2} = m\frac{\mathrm{d}^2y(x,t)}{\mathrm{d}t^2} + m\frac{\mathrm{d}^2y_0(x,t)}{\mathrm{d}t^2}$$

The variables, x and t, can be separated to render:

$$y(x,t) = \sum_{i=1}^{n}\sin\frac{i\pi x}{L}y_i(t)$$

Then, multiplying by $\sin k\pi x/L$, and carrying out the integration between 0 and L, the generalised coordinate corresponding to mode k is given by the equation:

$$y_k''(t) + \omega_k^2 y_k(t) = -\frac{2}{k\pi}\frac{\mathrm{d}^2y_{\mathrm{B}}}{\mathrm{d}t^2} = \frac{2\omega^2 A}{k\pi}\sin\omega t \qquad (71)$$

By direct comparison with the behaviour of a simple oscillator subjected to a harmonic force, one concludes that the amplitude of the permanent movement of the cable, for the mode k, is given by:

$$A_k = A\frac{2\omega^2}{k\pi\omega_k^2}H(\omega) \qquad (72)$$

where $H(\omega)$ is the classical amplification factor, figure 33, given by:

$$H(\omega) = \frac{1}{\sqrt{\left[1-\left(\frac{\omega}{\omega_k}\right)^2\right]^2 + \left[2\xi\left(\frac{\omega}{\omega_k}\right)\right]^2}} \qquad (73)$$

with ξ being the damping coefficient (ratio to critical) corresponding to the second term to be introduced in the equation:

$$2\xi\omega_k y_k'(t)$$

It is clear that significant vibrations can only develop when periods are very close, as shown by equations (69) and (70), which can be condensed as follows:

$$\frac{kA_{\mathrm{k}}}{A} = \frac{2}{\pi}\left(\frac{\omega}{\omega_k}\right)^2\frac{1}{\sqrt{\left[\left(1-\left(\frac{\omega}{\omega_k}\right)^2\right)^2 + \left(2\xi\left(\frac{\omega}{\omega_k}\right)\right)^2\right]}} \qquad (74)$$

equation (74) is displayed in figure 34 and table 2.

When the periods are different by less than 2%, the transverse displacement of an anchorage produces cable vibrations with amplitude which is at least seven times larger for mode 1. The amplitude should be divided by k for

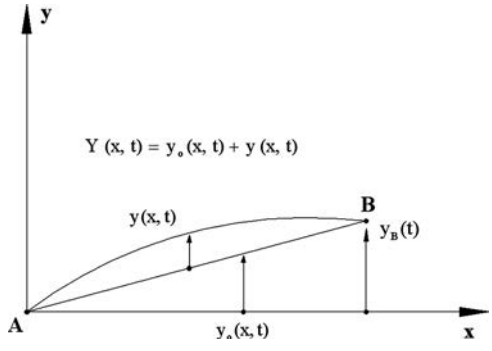

Figure 32. Analysis of transverse cable excitation.

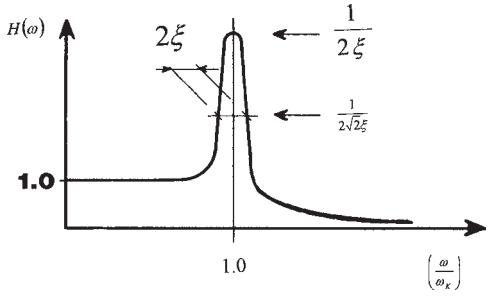

Figure 33. The amplification factor as a function of ω/ω_k.

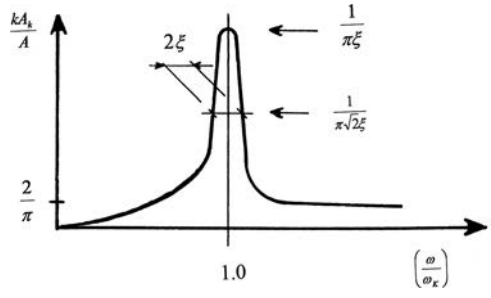

Figure 34. Vibration amplification in a stay cable.

the typical mode. Therefore 10 cm at the anchorage corresponds to at least 70 cm for cable vibration in mode 1, and to 35 cm in mode 2, etc. The most interesting result is that damping cannot reduce this effect, except at peak. In other words, the amplification is practically independent from the damping coefficient. This is a very significant consideration in the design process; if some stay cables are affected by parametric excitation, increasing damping would not be sufficient.

Now, the longitudinal excitation produced by the movement of the same anchorage in the cable direction, $u_B(t)$, is considered (figure 35):

$$u_B(t) = A \sin \omega t$$

Here, the tension variation produced by the cable elongation should be considered:

$$\Delta L = \int_0^L \sqrt{\left(1 + \frac{du(x,t)}{dx}\right)^2 + \left(\frac{dy(x,t)}{dx}\right)^2}\, dx - L$$

Table 2. Equation (74) at different levels of damping.

	$\xi = 0.001$	$\xi = 0.002$	$\xi = 0.003$
0.94	5,468	5,466	5,462
0.96	8,118	8,11	8,098
0.98	16,056	15,998	15,902
0.99	31,834	31,376	30,68
0.994	52,492	50,496	47,622
0.998	142,524	112,708	88,432
1.000	318,31	159,154	106,104
1.002	142,182	112,37	88,134
1.006	52,17	51,64	47,28
1.01	31,514	31,052	30,324
1.02	15,738	15,68	15,58
1.04	7,8	7,792	7,78
1.06	5,15	5,148	5,144

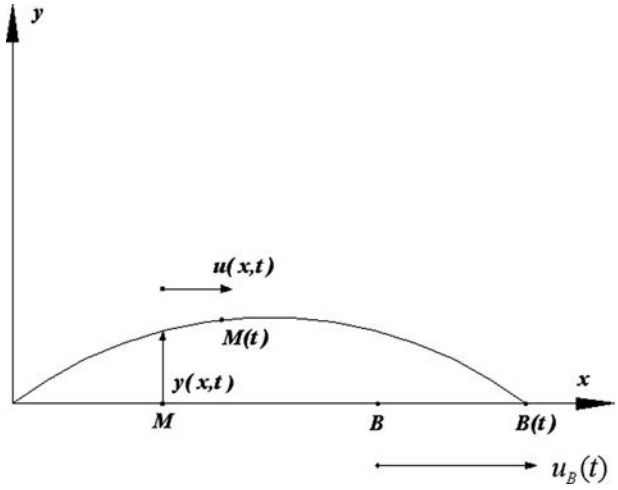

Figure 35. Analysis of a longitudinal cable excitation.

The displacement of a typical point is given by $u(x,t)$, and $y(x,t)$. It is clear that the only first-order term will come from the longitudinal displacement and therefore:

$$\Delta L = \int_0^L \left(1 + \frac{du(x,t)}{dx}\right) dx - L = u_B(t)$$

From the above relationship, one obtains:

$$\Delta F = \frac{ES}{L} A \sin \omega t$$

The following equation is given by the cable dynamic equilibrium:

$$(F + \Delta F)\frac{d^2 y(x,t)}{dx^2} = m\frac{d^2 y(x,t)}{dt^2}$$

By separation of the variables and using equation (10), one obtains:

$$y_k''(t) + \omega_k^2 \left(1 + \frac{ES}{FL} A \sin \omega t\right) y_k(t) = 0 \qquad (75)$$

The above formula, incorporating the damping factor, can be transformed into a classical Mathieu–Hill equation (Clément and Cremona 1996). It can be shown that there are two different types of resonance with a longitudinal excitation. Resonance that takes place at the same period, or frequency, is easily understood when considering the sag effect. The main type of resonance occurs with a period which is double of the excitation, or half of the frequency. Figure 36 shows the two instability zones, corresponding to the excitation period, T, or its double, $2T$. The main resonance modes for longitudinal excitation are displayed in figure 37.

More sophisticated analyses can be developed introducing the sag effect produced by the cable weight, and the elongation produced by the transverse displacement. However, the nature of the results would not vary.

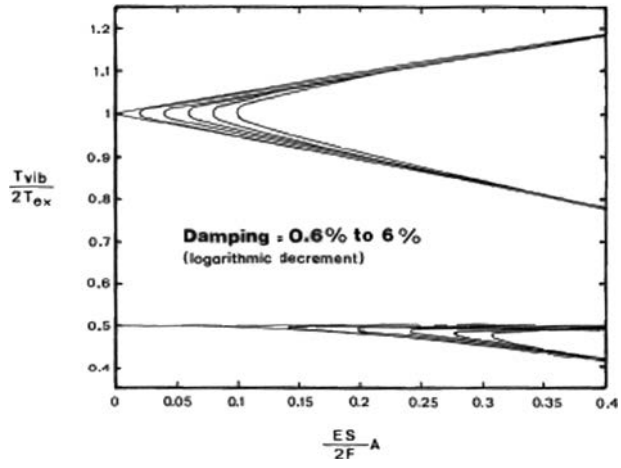

Figure 36. Zone of instability with a longitudinal excitation.

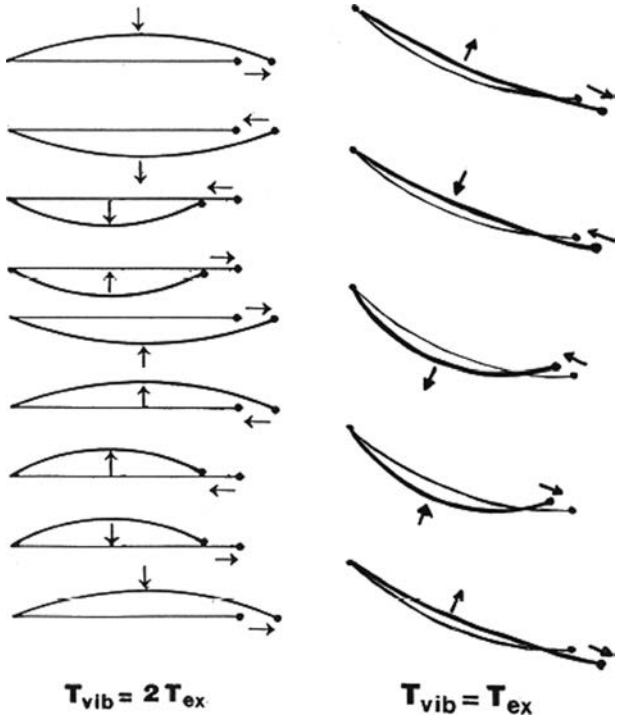

Figure 37. Main resonance modes for longitudinal excitation.

6.6 *Rain and wind-induced vibration*

One of the most significant problems is the phenomenon caused by rain and wind interactions, as demonstrated by many researchers (Hikami and Shiraishi 1988, Yamaguchi 1990, Flamand 1994, Saito *et al.* 1994, Geurts and Staalduinen 1999). In oblique wind conditions that tend to lift the cable, and in rainy weather, two water rivulets may run down the surface of the cable—at the lower part of the duct, and at the upper part of the duct where the rivulet has a dynamic equilibrium. The equilibrium is achieved under the combined effects of gravity, capillary and wind forces which oppose gravity forces when the angle of azimuth of the wind is in the convenient range. The water rivulets change the effective shape of the cable, and thus aerodynamic forces; and they move as the cable oscillates, causing cyclical changes in the aerodynamic forces which increase oscillations in given conditions. This type of instability is directly dependent on the existence of the upper rivulet. Without the upper rivulet, there is no cable vibration, and vibrations develop when the water rivulet flows in a critical zone of the upper surface of the cable.

From the literature cited above, rain and wind-induced vibrations can develop in different weather conditions. The rain intensity is not of major concern; a strong drizzle can produce these vibrations. Heavy rain does not seem so unfavourable, because the quantity of water could exceed the capacity of the cable to maintain a water rivulet on its upper surface. The vibrations have mainly been observed on cables with ducts in high-density polyethylene (HPED). It is worthy to note that the capillary action plays a role and also the nature of ducts; however, it should be noted that most cables are now placed in HDPE ducts. In addition, the vibrations which occurred during the erection of the Brotonne Bridge in 1977–1978, before the installation of dampers at the lower anchorages, could be attributed to the combined effects of rain and wind. The ducts were painted steel pipes; the same could be said for the bridge at Wandre over the river Meuse, where ducts are in stainless steel. The tests made by the CSTB for the Normandie Bridge reproduced some of the Japanese results (figure 38). If the ducts are smooth, the upper rivulet cannot exist and the cable oscillations do not develop. Jacques Biétry and Olivier Flamand had to 'dirty' the cable surface, with some carbon soot, to install the water rivulet and the corresponding vibrations (figure 39).

The diameter of ducts for which such vibrations were observed is in the range of 140–225 mm. Wind tunnel tests in Japan were made for relatively smaller cables. However, some vibrations observed on bridges (such as for the Glebe Island and Erasmus bridges) correspond to larger diameters. These cable vibrations only develop for oblique winds, with an angle of azimuth between 30 and 80° according to some authors; or between 20 and 60° according to others. It should be noted that vibrations mainly take place due to winds which tend to lift the cables. Rain and wind-induced cable vibrations have been observed for wind velocities between 6 and 18 m s^{-1} according to some authors. The majority of vibrations correspond to wind velocities between 8 and 12 m/s. Referencing the reduced velocity, U_R, given by:

$$U_{\mathrm{R}} = \frac{U}{ND} \tag{76}$$

Figure 38. Stay cable tested by the CSTB in the Jules Verne climatic wind tunnel.

where U is the wind velocity, N is the vibration frequency, and D is the duct diameter, the vibrations develop between 20 and 90 m/s (Hikami and Shivaishi 1988, Saito *et al.* 1994, Flamand 1994). These values are generated for Reynolds numbers in the range of 6×10^4 and 2×10^5. The frequency of the observed vibrations generally ranges between 1 and 3 Hz according to some investigators, and between 0.60 and 3 Hz according to others. Most frequent vibrations develop at about 1.0 Hz. Recorded vibrations are mainly vertical, in perfect agreement with the idea that these vibrations come from the correlation between the vertical movements of the cable and the displacements of the water rivulets on the cable surface. Transverse movements could also be associated with the vertical movements. The amplitude of vibrations which have been produced in wind tunnels is about twice the cable diameter. However, in some bridges, vibrations could reach several metres, as was observed on video records at the Burlington Bridge and the Glebe Island Bridge. According to some information, the extreme case of cable vibrations took place at the Second Severn crossing. This might have been the case; probably dueÂto other reasons of cable vibrations that amplified the combined effects of rain and wind. Figure 40 displays the vibration amplitude as a function of the wind velocity.

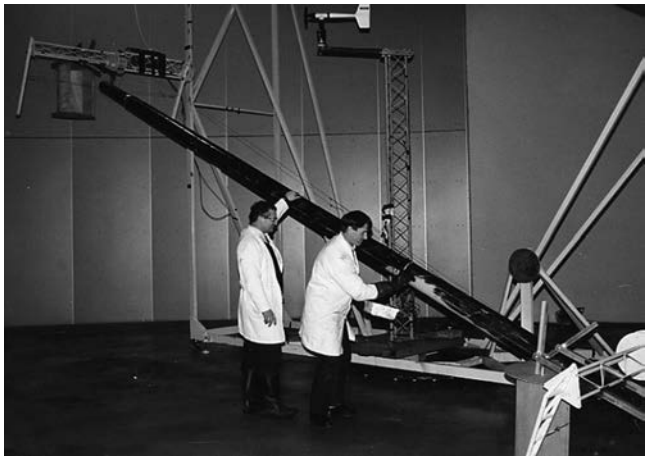

Figure 39. Preparation of the test, with carbon soot on the duct.

These vibrations mainly occur for bridges built in a flat topography, or over a wide waterway. It is interesting to note that heavy wind turbulence would prevent or limit the organized vibrations of water rivulets, and thus cable vibrations.

7. Cable/structure interaction

7.1 *Structural analyses*

Classical analyses of cable-stayed bridges are performed with linear models in which stay cables are represented by straight elastic members, without inertia, and without

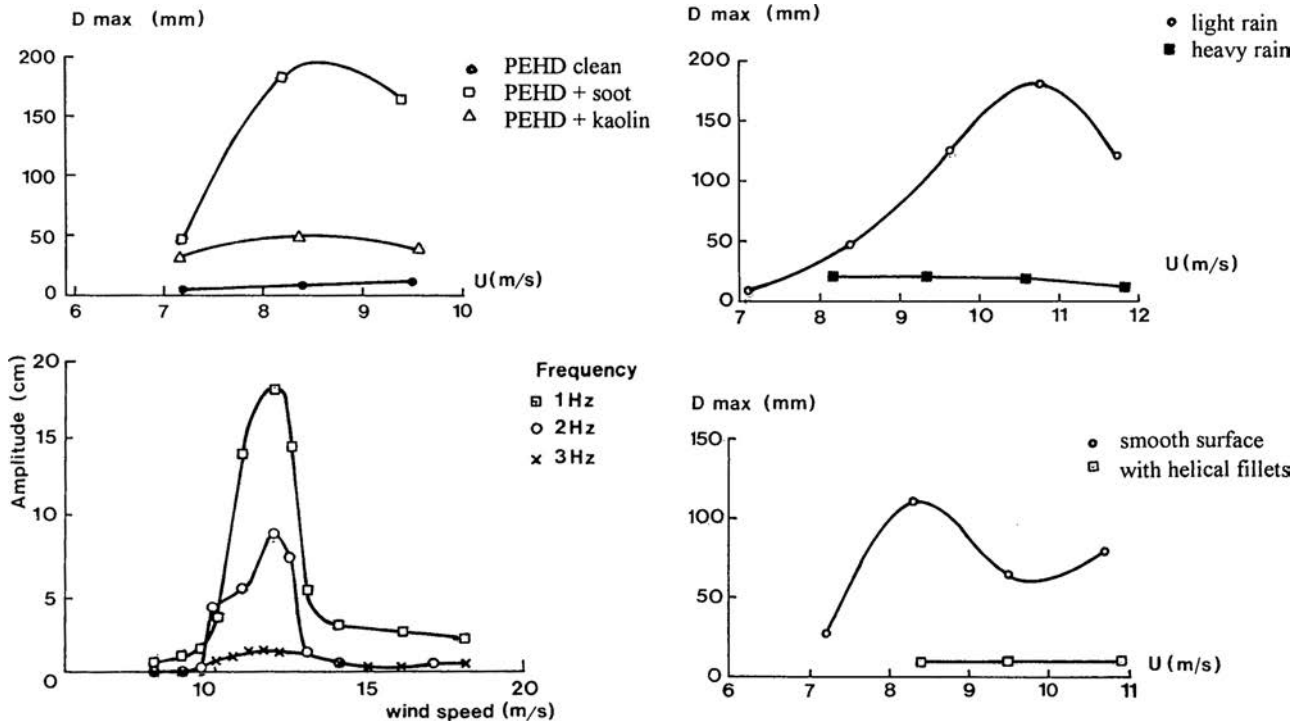

bending moments at their anchorages, in deck or towers. Their mass is introduced in the structure by halves at their two anchorages as shown earlier. As a consequence, vibration modes are separated into two independent categories. The first is 'structural' modes, which are given by the dynamic linear analysis of the structure, in which stay cables are modelled by elastic bars without mass. The second category is 'cable' modes, evaluated by an independent analysis of stay cables, one by one supposing that its two anchorages are fixed. This separation is extremely efficient for the structural analysis, allowing for a simple, rapid and safe evaluation of forces. It is also extremely efficient for detecting possible interactions between stay cables and the structure, when some 'structural' frequencies are close to some 'cable' frequencies. Parametric excitation of the corresponding stay cables from the structure vibrations is very likely. As demonstrated in section 6.5, the amplitude of the stay cable vibrations may be very high. It is clear, however, that there is an interaction between the 'structure' and the stay cables. It is only possible to have a precise evaluation of this interaction with a more complex model in which stay cables are represented with their mass distributed along their length; a model which will also verify sag effects in stay cables. Such computations lead to a very high number of vibration modes. For instance, the author had to analyse 300 modes for the Normandie Bridge in order to identify the main 'structural' modes in the complete series. It is therefore necessary to develop some techniques to recognise the different types of modes. The identification is only possible when all data corresponding to the following three analyses are available:

- the classical linear analysis, leading to the structural modes,
- the analysis of the stay cable frequencies, supposing that they are independent, and
- the detailed dynamic analysis with stay cables represented with their distributed mass.

The frequencies and modes of the detailed dynamic analysis should be compared to the results of the first two analyses. The key elements of comparison are the values of frequencies, the mode shapes, the generalised masses and above all the number of modes, corresponding to 'degrees of freedom'. If one considers the example of a bridge with a unique tower, provided with two planes of stay cables and with backstays different from the stay cables in the main span, the following modes have to be identified in the detailed analysis.

- Pure 'structural' modes, when they are completely separated from 'cable' modes; in these modes, of high generalised mass, some stay cables may move, but not very much.
- Pure 'cable' modes, but in groups. In this example, for each given pair of stay cables, either in the main span or in the side span, and for each mode order k, one should identify:
  - two lateral modes, which can be separated in a symmetric and an antisymmetric mode if the structure is perfectly symmetrical, and
  - two vertical modes which can be separated in the same way; with a slightly different frequency for mode 1 due to sag effects, and with almost the same frequency for higher modes, finally leading to a group of four modes with the lateral modes. These modes have a very limited generalised mass and show large displacements of stay cables, with no or very small displacements of deck and towers.
- Mixed modes, when a group of cable modes, two or four in this example, depending on the mode order of the cables, interacts with a structural mode.

The analyses performed, by Mr Nauta for the Erasmus Bridge in the Netherlands verify this type of interaction, between two 'structural' modes and four stay cables. The first vertical vibration mode has a period, when computed with cables modelled by simple elastic bars, very close to the first natural period of cables 10 and 11. The combination results in nine modes in the detailed computations made with DIANA (figure 41), with these two cables modelled with their mass and sag effect, as shown in tables 3 and 4. Since there are in fact four cables, two cables 10 and two cables 11, vibrating vertically and laterally, each cable of each pair has been modelled with a specific tension evaluated from measures at the construction time. It is clear that modes 1–4 correspond to lateral vibrations of cables 10 and 11, sway or balancement, and modes 5–9 combine vertical vibrations of deck and cables 10 and 11. The values of generalised masses, and the aspect of modes, show that modes 5 and 9, but mainly 5, concentrate the larger part of the mass. The normalisation of modes corresponds to a larger displacement component equal to 1.0 m. Figure 9 demonstrates the nine modes combining the first structural vertical mode and the first vibration mode of stay cables 10 and 11.

The combination of structure and cable modes can be more complex, as shown by the combination of structural mode 4 (sway 1) and of mode 2 in cables 10 and 11. Some modes are only concerned with vertical cable vibrations; sometimes limited to one cable, or vertical and lateral vibrations of cables, with some participation of the deck (lateral vibrations). Mode 20 is the most structural.

The author performed a similar analysis for the Normandie Bridge, but with all the stay cables modelled by Alain Morisset with their mass and with the aiguilles (or cross cables). For lateral vibrations four modes were produced in each group in the main span (as well as in

Table 3. Simplified analysis of structure and stay cables.

Structural modes			Cable modes		
Mode	Period	Type	Cable	Period	Type
1	2.2173	Vertical 1	11 west	2.479	Lateral 1
4	1.2071	Sway 1	10 west	2.448	Lateral 1
			11 west	2.2428	Vertical 1
			10 west	2.1994	Vertical 1
			11 west	1.2392	Lateral 2
					Vertical 2
			10 west	1.2240	Lateral 2
					Vertical 2

Table 4. Detailed computations of two cables modelled with their mass and sag effect.

Mode	Period	Generalised mass (10^4)	Type
1	2.4361	1.3298	
2	2.4337	1.2962	Lateral modes of cables
3	2.4213	1.4280	10 and 11
4	2.4195	1.3922	
5	2.3436	6.2036	
6	2.2528	2.0644	Vertical modes of deck
7	2.2114	2.6274	and cables 10 and 11
8	2.1988	1.9332	
9	2.1277	3.4317	
12	1.2300	4.3706	
13	1.2167	1.7689	
14	1.2167	1.4774	Mainly cable vibration
15	1.2161	2.2752	with small deck
16	1.2133	3.4686	vibration (modes 12–16)
17	1.2098	1.6597	
18	1.2095	1.3885	
19	1.2079	3.0091	
20	1.1869	10.501	Transverse deck and cable vibration

the side spans) for each pair of stay cables, which can have symmetrical and antisymmetrical shapes, as shown by figure 42, the first symmetry corresponding to the longitudinal axis of the bridge, and the second to the transverse horizontal axis at mid-span.

It should be noted that the precise interaction between structure and cables cannot be predicted when frequencies of structure and cables are almost the same, since the result is highly dependent on the difference which cannot be predicted with accuracy. The uncertainties in the cable tension, or in the deck inertia, can be much higher than needed to predict accurately the 'combined' modes. This is more pronounced at the design stage than after erection when measures can reduce the uncertainties. In this situation, it is absolutely impossible to predict the exact scale of the possible influence of parametric excitation and the designer can have only two options. First, to wait for erection, observe the real bridge behaviour and then take proper countermeasures. Alternatively, if it is thought that there is a major risk, the frequencies have to be separated to ensure that parametric excitation would not take place.

7.2 *A simple interaction model*

For a real structure, or in the structural analysis when the structure is represented by a detailed model, with cables represented by their mass and sag effect, the parametric excitation cannot be considered as an excitation of the cable ends. It becomes necessary to develop a direct analysis of the global structure vibration, excited by vortex shedding, buffeting or traffic. Clearly, the analysis becomes much more difficult and needs the use or the development of specific software. The author analysed the influence of Von Karman vortices on the pylons of the Millau Viaduct, and the possible parametric excitation of the two longer stay cables in each cantilever. Vincent de Ville built a finite element model of a pylon with a unique stay cable which demonstrated two results. First, when there is a perfect identity between the independent vibration periods of tower and cable, the interaction separates the two modes into a symmetrical one and an antisymmetrical one with different frequencies. The influence of vortex shedding on the system is much lower than the effect of parametric excitation on the stay cable derived from the estimated movement of the pylon, which is reduced.

To control these results, it is proposed to use a simplified model with two degrees of freedom. The model is composed of a pylon, a stay cable of length L, at an angle α with the horizontal and a tension force, F (figure 43).

Assume that the pylon has a mass M_0, concentrated at the anchorage of the stay cable, and rigidity, R_0. The total mass of the stay cable, mL, is introduced at both anchorages and at mid-span; in the tower $mL/4$, at the fixed lower anchorage $mL/4$, and at mid-span $mL/2$.

The anchorage of the stay cable at the pylon has a lateral displacement, Y, while the lateral displacement corresponding to the node at mid-span of the stay cable is given by $(\frac{Y}{2} + y)$. The relative movement, y, and the angles, θ and φ are shown in figure 44, where:

$$\mathrm{tg}\theta \approx \theta = \frac{Y}{L\cos\alpha}; \qquad \mathrm{tg}\varphi \approx \varphi = \frac{2y}{L\cos\alpha}$$

The horizontal transverse force produced on the pylon by the stay cable is given by:

$$F\cos\alpha\sin(\theta - \varphi) = \frac{F}{L}(Y - 2y)$$

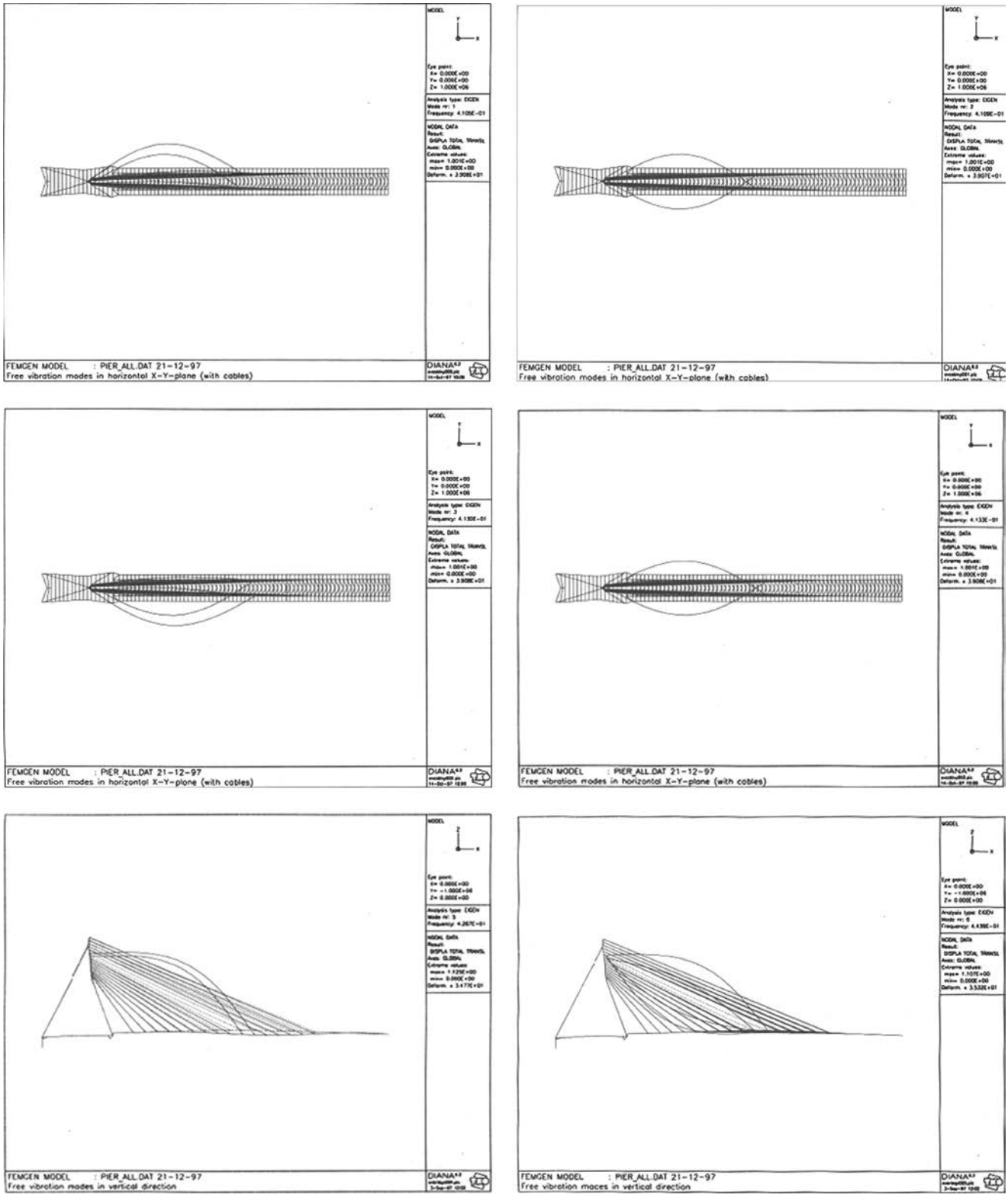

Figure 41. The nine modes combining the first structural vertical mode and the first vibration mode for stay cables 10 and 11.

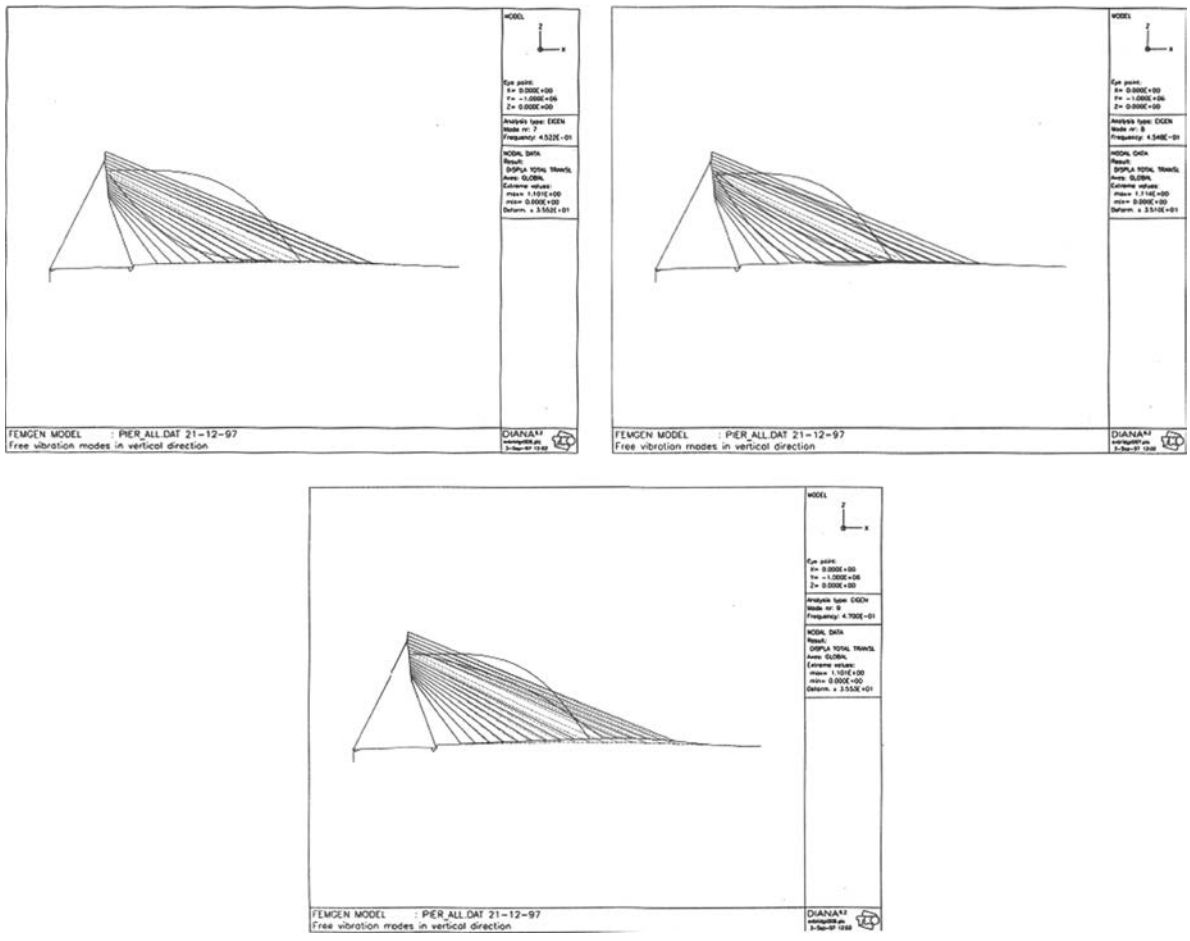

Figure 41. (*continued*)

The tension in the stay cable produces a force in the node at mid-span given by:

$$2\,F\cos\alpha\sin\varphi = \frac{4F}{L}y$$

The equilibrium of the central node of the stay cable leads to the equation:

$$\frac{mL}{2}\left(\frac{Y''(t)}{2} + y''(t)\right) = -\frac{4F}{L}y(t)$$

This can be reduced to:

$$\frac{1}{2}Y''(t) + y''(t) + \omega^2 y(t) = 0$$

where ω is the pulsation of the cable mode, which can be written as follows:

$$\omega^2 = \frac{8F}{mL^2}$$

The pylon equilibrium is given by the equation:

$$\left(M_0 + \frac{mL}{4}\right)Y''(t) + R_0\,Y(t) = -\frac{F}{L}[Y(t) - 2y(t)]$$

In turn, this can be reduced to:

$$Y''(t) + \omega_i'^2\,Y(t) - \frac{mL\omega^2}{4M}y(t) = 0$$

with:

$$\omega_i'^2 = \frac{R_0 + \frac{F}{L}}{M_0 + \frac{mL}{4}}$$

and:

$$M = M_0 + \frac{mL}{4} = \frac{m_i}{[\varphi_i(h)]^2} - \frac{mL}{4}$$

The parameter, m_i, is the generalised mass of the pylon mode in the structure evaluated from a linear analysis. It automatically includes half the weight of the stay cable; where φ_i (h) is the modal transverse displacement of the pylon at the anchorage level. The

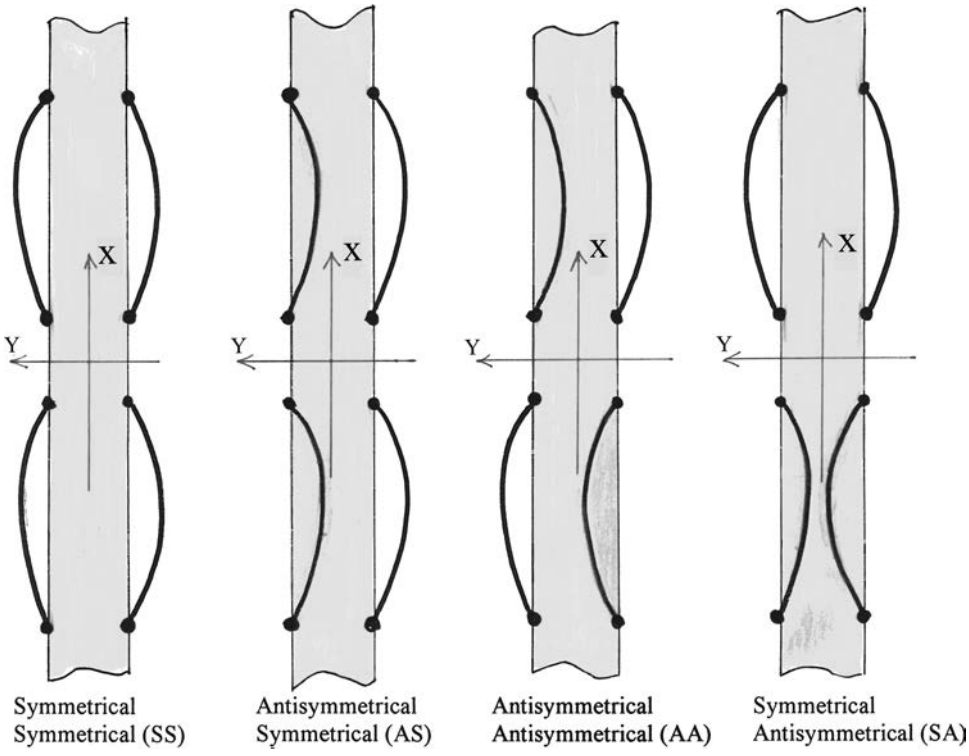

Figure 42. Symmetry of lateral cable modes at the Normandie Bridge.

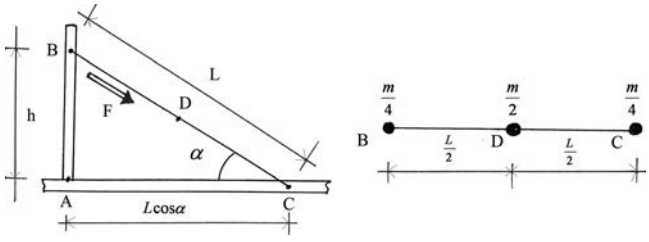

Figure 43. Simplified model for the interaction between the tower and stay cable.

pulsation of the pylon mode, ω_i, which includes the stay cable pulling effect, is then given by:

$$\omega_i^2 = \frac{R_0 + \frac{F}{L}}{M_0 + \frac{mL}{2}}$$

From the above expression, one obtains:

$$\omega_i'^2 = \left(1 + \frac{mL}{4M}\right)\omega_i^2 \tag{77}$$

The two equilibrium equations can be grouped as follows:

$$\begin{Vmatrix} 1 & 0 \\ \frac{1}{2} & 1 \end{Vmatrix} \begin{Vmatrix} Y'' \\ y'' \end{Vmatrix} + \begin{Vmatrix} \omega_i'^2 & -\frac{mL\omega^2}{4M} \\ 0 & \omega^2 \end{Vmatrix} \begin{Vmatrix} Y \\ y \end{Vmatrix} = 0$$

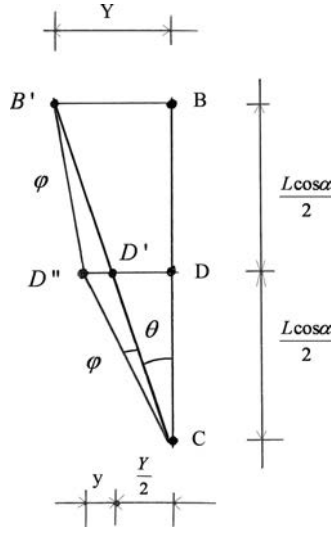

Figure 44. Schematic of a simplified interaction model.

The eigenvectors, $\begin{Vmatrix} \alpha \\ \beta \end{Vmatrix}$, should be found; such that:

$$\begin{Vmatrix} Y'' \\ y'' \end{Vmatrix} = -\Omega^2 \begin{Vmatrix} Y \\ y \end{Vmatrix} = -\Omega^2 \begin{Vmatrix} \alpha \\ \beta \end{Vmatrix}$$

The result is expressed by:

$$\Omega = \frac{1}{\sqrt{2}} \times \sqrt{\left[\omega_i'^2 + \left(1 + \frac{mL}{8M}\right)\omega^2\right] \pm \sqrt{\left[\omega_i'^2 + \left(1 + \frac{mL}{8M}\right)\omega^2\right]^2 - 4\omega_i'^2\omega^2}} \tag{78}$$

Equation (78) clearly demonstrates the separation of the two modes. The closest solutions are obtained at resonance when:

$$\omega = \omega_i'$$

The solutions are then given by:

$$\Omega = \omega_i\left(1 + \frac{mL}{4M}\right)\sqrt{\left(1 + \frac{mL}{16M}\right) \pm \sqrt{\frac{mL}{8M} + \left(\frac{mL}{16M}\right)^2}} \tag{79}$$

8. Countermeasures

In this section, three different solutions will be presented to eliminate or reduce cable vibration; namely, increased damping, use of shaping ducts, and installation of cross cables.

8.1 *Increased damping*

The classical solution is to increase damping in cables, as was done for the Brotonne Bridge and the bridges at Wandre and Ben Ahin in Belgium, with the installation of hydraulic dampers at the lower anchorage of cables.

Figure 45. A damper at the Iroise Bridge over the River Elorn.

The most efficient systems are made of two dampers at an angle transversally, as for the Brotonne Bridge and the Iroise Bridge over the river Elorn between Plougastel and Brest (figure 45). Some suppliers tried to design dampers of a much smaller size, installed as rings between the cable proper and a reservation pipe imbedded in concrete, or extending the steel or concrete structure. These 'ring dampers' were just a neoprene ring in the first applications, such as initiated by VSL. Much more efficient systems have been developed with viscous products, as those used by Freyssinet for the Vasco de Gama Bridge (figure 46) and by other suppliers

The design of dampers needs a full paper, which should include the definition of the dampers' rigidity and damping characteristics to produce the desired damping coefficient at the desired frequencies, and temperature. Suppliers usually present design criteria or diagrams, which are generally built in such a way to protect the supplier's know-how, and therefore they cannot be fully understood by bridge engineers.

An increased damping is efficient to reduce almost all types of cable vibration, except for parametric excitation as demonstrated earlier. From the Japanese literature, it is

Figure 46. A damper at the Vasco de Gama Bridge (photo courtesy of Freyssinet).

considered that damping can eliminate rain and wind-induced vibrations when the damping coefficient (ratio to critical) is higher than 0.5%, or when the logarithmic decrement is higher than 3%. The efficiency of the dampers depends on their location: they have to be at some distance from the anchorage; external hydraulic dampers have to be as perpendicular to the stay cable as possible. The dampers shown in figure 47 could not prevent significant vibrations since they were close to the anchorage, and at an unfavourable angle.

8.2 *Shaping ducts*

The second type of remedy for cable vibrations has been developed recently in Japan, and for the Normandie Bridge with a different pattern. It consists of shaping ducts to eliminate rain and wind-induced vibrations. In Japan, the ducts of the Higashi-Kobe Bridge received deep longitudinal channels to drive water down without possible transverse movements (figure 48). The drawback is a dramatic increase in the drag coefficient, from 0.50 or 0.60 for overcritical values of the Reynolds number to about 1.35.

The problem of rain and wind-induced vibrations was questioned for the Normandie Bridge by the Danish Contractor Monberg and Thorsen and its consultant Cowi. Tests were organised in the Jules Verne climatic wind tunnel of the CSTB, at Nantes, to compare different possible solutions. The selected solution, which has been patented by Freyssinet, consists of providing the ducts with two helical filets, only 1.3 mm deep, with a pitch length of 60 cm each (figure 49). These helical filets destroy the coherence of the vibrations of the water rivulets flowing along the ducts and thus cable vibrations, as suggested by the Danish Maritime Institute. The author insisted on the limitation of the drag coefficient, to limit wind forces on the bridge. With the 1.3 mm deep filets, the drag coefficient only reaches 0.63. It also appears that the drag coefficient is constant on a larger interval of the Reynolds number. For the Tatara Bridge in Japan, a new type of duct shaping was developed, with a distribution of dimples (figure 50). It would be extremely interesting to observe the performance of this new design, particularly since the Tatara Bridge has no cross cables.

Figure 47. Example of dampers installed too close to the anchorage, which could not prevent cable vibrations.

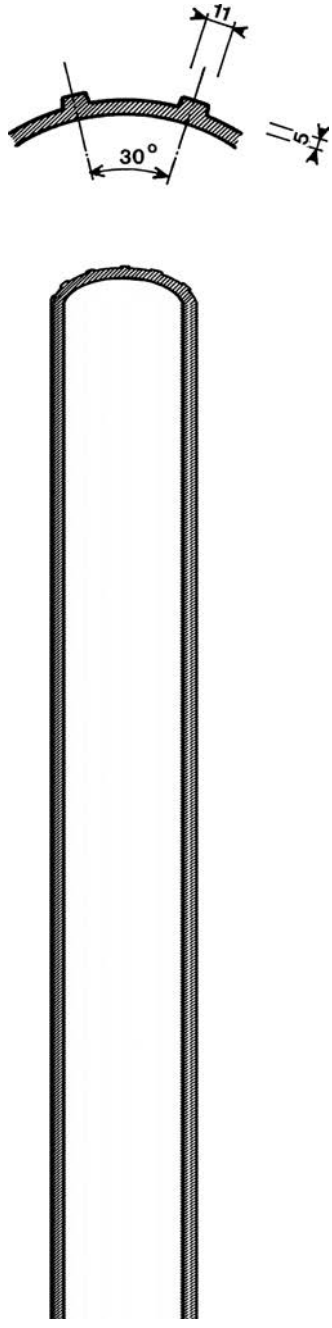

Figure 48. Longitudinal channels of the ducts at the Higashi-Kobe Bridge.

As mentioned earlier, these different types of duct shaping have been developed to prevent rain and wind-induced vibrations. Nevertheless, when the ducts were installed on the Normandie Bridge cables, sooner than expected to stop breathing of strands which revealed extremely disagreeable, all cable vibrations disappeared. This type of shaping may also increase aerodynamic damping; but no test was made to check the validity of that.

Figure 49. A duct of the Beaucaire Bridge with the helical filets.

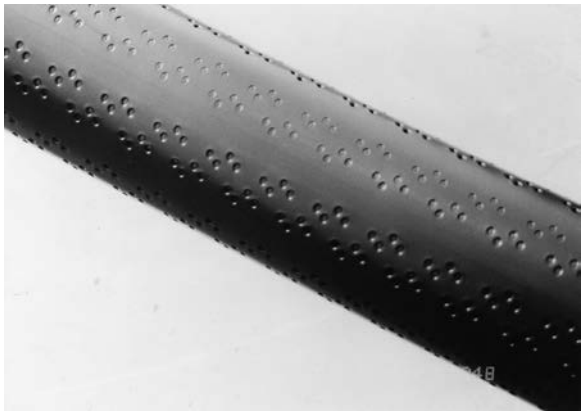

Figure 50. Dimples on the ducts of the Tatara Bridge in Japan (photo courtesy of the Honshu-Shikoku Bridge Authority).

8.3 *Cross cables (aiguilles)*

The last solution presented in this paper is the installation of interconnecting ropes, or cross cables. The author proposed the French word 'aiguilles' to describe the cross cables installed on the Normandie Bridge. The concept of cross cables has first been developed to increase the rigidity of the cable-stayed system in cable-stayed bridges with very long spans. The idea has been proposed by Fritz Leonhardt for his proposal for the Messina Straight crossings, but was never used in practical applications. The first practical application was at the Farö Bridge in Denmark (figure 51). Some of the longer cables were prone to vibrations, that were attributed to the combined effects of rain and wind. The amplitude of these vibrations was much lower than those that occurred at many other bridges. Cowi Consultants proposed the use of small aiguilles, tying the longer cables only, with no connection to the deck or pylons. The system was successful in suppressing the vibrations; however, after the design of the Normandie Bridge, the author learned that one of the cross cables at the Farö Bridge broke. The cross cables were replaced by stronger ones, with higher tension force and the system has been reported in satisfactory conditions.

Another application is used in the Japanese bridges, where the cable-stayed system is made of a series of pairs of cables. Cross cables have been installed to avoid wake effects in twin cables. The system was used for the two cable-stayed bridges on the Kojima-Sakaide route of the Honshu-Shikoku project, figures 52 and 53, at the Yobuko Bridge during construction and for other bridges later. The system demonstrated efficiency even with a reported break of one of the cross cables on the central line of the Honshu-Shikoku project. The author has learned from engineers at the Honshu-Shikoku that a series of cross cables have been replaced afterwards by stronger cables with a higher tension.

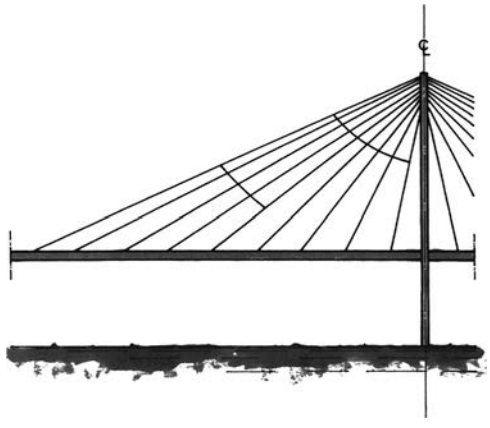

Figure 51. Cross-cables at the Farö Bridge.

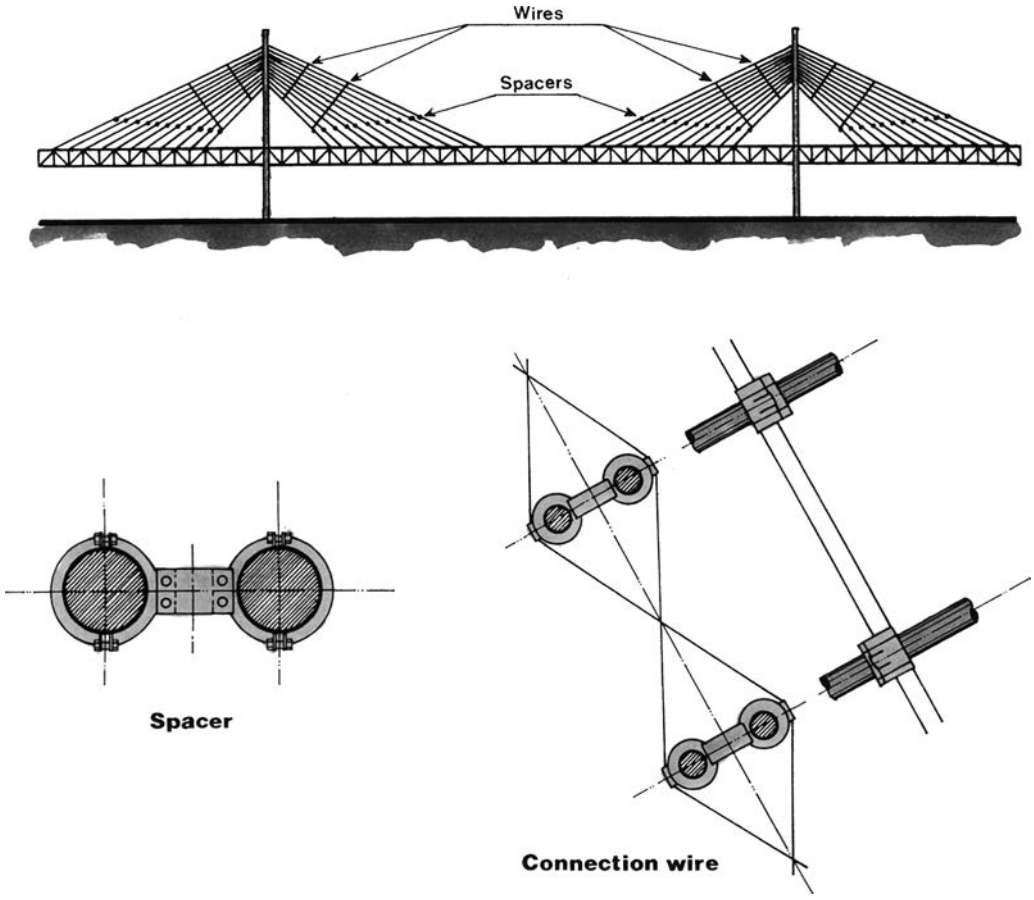

Figure 52. Cross cables for the cable stayed bridges on the Kojima-Sakaide route.

Figure 53. View of the aiguilles on the Kojima-Sakaide route.

The last application of cross cables, reported in this paper, has been developed for the Normandie Bridge (figure 54). During the design of the bridge, the author noticed that the first vibration period of cables was in the same range as the 'structural' vibration periods, vertical modes 1, 2 and 3. The author therefore concluded that the deck vibrations could initiate significant parametric excitation in the cables. The decision was made to install aiguilles in order to drastically change the vibration periods of cables, at least for the vertical modes, to have them out of the range of the structure main vibration periods (figures 55 and 56). It was also decided to install robust cross cables with high tension to avoid shocks during high winds. Additionally, the cross cables were provided with high internal damping. This last addition was inspired by the suspenders of suspension bridges designed by Freeman, Fox and Partners, in which ropes are made with a short pitch length providing high damping and low fatigue resistance. Freyssinet developed a better solution with ropes provided by Bridon. The Freyssinet/Bridon design provides high internal damping and a satisfactory resistance to fatigue.

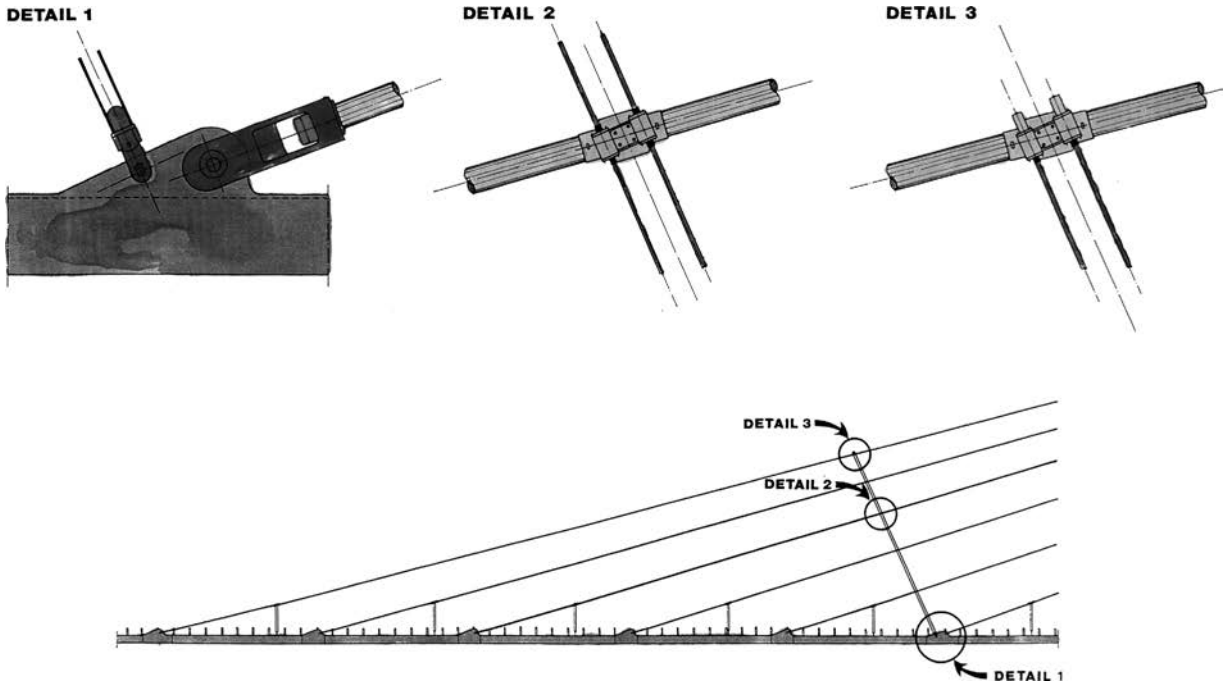

Figure 54. Details of cross-cables at the Normandie Bridge.

Figure 55. Installation of the aiguilles at the Normandie Bridge.

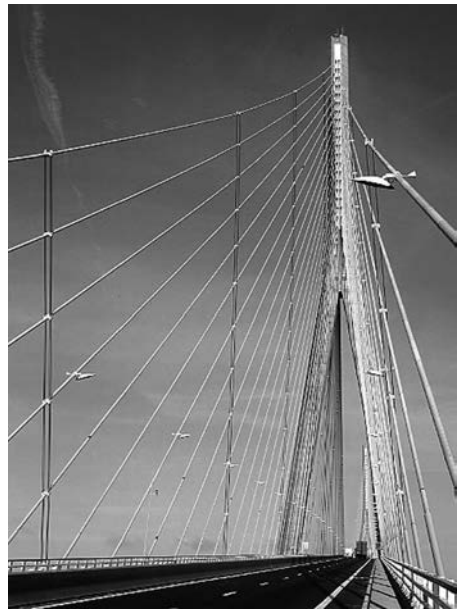

Figure 56. Duct and cross-cables at the Normandie Bridge (photo courtesy of Freyssinet).

From this series of applications, it is shown that cross cables can be used to eliminate or reduce different types of cable vibrations. It must be noted that the number of cross cables required to stop rain and wind-induced vibrations can be high. The reason is that it is necessary to increase the natural frequencies of cables above 3 Hz to ensure the effectiveness of the cross cable in suppressing cable vibrations. The number of cross cables could be reduced if their damping effect would provide the desired effect in reducing the cable vibrations.

Aiguilles can also be used to stop or limit cable vibrations which appear in a bridge after construction.

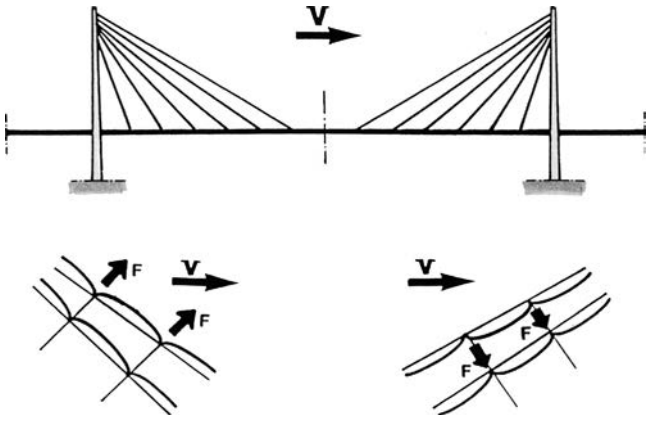

Figure 57. Evaluation of wind effects on stay cables, and cross-cables.

However, this leads to changes to the cable geometry due to the tension in the newly installed cross cables. The angle between the deck and the cables is reduced, and the tension in the cables is increased. At the same time, moments are slightly changed in the deck and pylons. As a result of the change in the angle between the deck and cables, and also between the cables and towers, some local bending is introduced in the cables at their connections to the deck and towers. These effects could be limited if the cables were properly designed, with an attachment at some distance from the anchorage. Due to the seriousness of the problem if bending effects reach the cable anchorage itself, this situation should be avoided.

The author was consulted on cable vibration problems at two large cable-stayed bridges. In one case, it has been decided to postpone the installation of cross cables or of any other countermeasures. It would be interesting to know the condition of the bridge in the long term, to evaluate the real danger of rain and wind-induced vibrations with respect to fatigue. Cable vibrations, for the other case, according to a wind engineering expert were produced by the combined effects of rain and wind, or most probably by cable-galloping under oblique winds. In other words, it was the wind expert's opinion that it is a case of aerodynamic instability of cables with oblique winds. The author's opinion was different; although recognising the fact that the larger cable vibrations occurred when it was raining, the author suggested that the vibrations could have been produced, at least partly, by deck vibrations. Deck vibrations are induced either by vortex shedding, as evident by the laminar winds in the same range of wind velocities, or by buffeting in oblique winds which were observed in the wind tunnel with a full aeroelastic model at the same wind velocities. Nevertheless, it was agreed that the installation of cross cables was the best solution. However, despite the author's recommendations, the cross cables were made of standard auto-protected strands which have an extremely low damping. To the author's knowledge, no significant cable vibrations were recorded after the installation of cross cables. However, significant vertical vibrations of the deck were observed. The deck vibrations were much larger than those observed before the installation of cross cables. The information received is that the deck vibrations were induced by vortex shedding on the structure itself which had been underestimated. These deck vibrations have been produced for the same wind velocities as for the cable vibrations observed previously, but for winds which were almost perpendicular to the bridge. It should be noted that the information received regarding the deck vibrations were not properly documented. The possible differences in the angle of azimuth, and the lack of precise documentation of the problem precludes any serious conclusions. It is the author's opinion that the stay cables, by their intense vibrations, were previously acting as dampers for the deck movements. When cable vibrations were suppressed by the cross cables, without the introduction of an additional damping, the damping of deck vibrations by the stay cable oscillations has vanished. Thus the amplitude of deck vibrations increased significantly. The author learned that the bridge superstructure has been equipped with baffles to prevent its vibrations. This measure has demonstrated satisfactory performance, though some cross cables have later failed.

8.4 *Design of cross cables*

The main goal of cross cables is to change the natural frequencies of the main cables, for vertical vibrations, in a manner which depends on the number of cross cables and their rigidity. The area of the cross cable cross-section and their tension force must be carefully selected so that stresses are acceptable under extreme effects produced by traffic, by wind-induced vibrations in the deck and pylons, and by the direct action of wind on cables. At the same time, the initial tension in the cross cables must be high enough that the tension cannot decrease to zero under the same extreme effects mentioned above. Of course, the system would remain stable, even if computations become more complex, if some cross cable segments become completely de-tensioned under extreme effects; but it would produce shocks in the cross cables segments which are de-tensioned and re-tensioned, which could lead to cross-cable ruptures, such as those experienced at the Farö and Honshu-Shikoku bridges. It is therefore imperative to include the cross cables in the full structural model of the bridge to study the effects of traffic loads on the cross cables. It is also essential to evaluate the effects of the extreme structure buffeting in cross cables. This is not so easy, due to the fact that the software packages used for the analysis of dynamic response to turbulent winds are not, generally, adapted to the definition of a complete structural

model, with the mass of the stay cables and the aiguilles. A simplified method can be developed as was done for the Normandie Bridge. Each main vertical mode (1, 2 and 3 at least) can be modelled by a static load, reproducing the deflection shape and scaling the extreme modal effect for the reference wind velocity. These static loads are introduced separately, or combined to represent the effects of a quadratic combination, on the complete bridge model, including cross cables of course, to analyse the resulting tensions.

The most unfavourable wind action on cross-cables is produced when the wind blows in the bridge longitudinal plane (figure 57). When a plane of stays is lifted by the wind, increasing tension in cross cables, another plane of stays is pushed by the wind, decreasing the tension in cross cables. The turbulent wind action is usually divided into two parts. First, the effect of the average wind velocity, which is a purely static action. Second is the effect of the wind turbulence which cannot be extreme on all stay cables at the same time and needs to be analysed considering spatial correlation. It should be noted that it is much more difficult to separate the dynamic effects into different 'modes' to be quadratically cumulative.

For the analysis of the Normandie Bridge, the author considered that extreme effects could be evaluated from the action of the average wind velocity multiplied by a dynamic amplification factor of 3.0. It is worth noting that Jacques Bietry has recently developed a more precise theory for the evaluation of extreme effects on cross cables.

Bibliography and References

Clément, H. and Cremona, Ch., *Etude mathématique du phénomène d'excitation paramétrique appliqué aux haubans de pont*. Laboratoire Central des Ponts et Chaussées. Série Ouvrages d'Art OA 18, Paris, Janvier 1996.

Davenport, A., A simple representation of the dynamics of a massive stay cable in wind, in *Proceedings of the International Conference on Cable-stayed and Suspension Bridges (AFPC)*, Deauville, 1994, Volume 2, pp. 427–438.

FHWA/HNTB. *Wind Induced Vibration of Stay Cables*. Interim Final Report, No. RI98-034 RDT05-004, February 2005.

Flamand, O., Rain/wind-induced vibration of cables, in *Proceedings of the International Conference on Cable-stayed and Suspension Bridges (AFPC)*, Deauville, 1994, Volume 2, pp. 523–531.

Geurts, C.P.W. and Staalduinen, P.C., Estimation of the effects of rains-wind induced vibration in the design stage of inclined stay cables. In *Wind Engineering into the 21st Century*, edited by Larsen, Larose and Livesey, pp. 885–892, 1999 (Balkema: Rotterdam).

Haubans. *Recommandations de la commission interministérielle de la précontrainte*, Novembre 2001 (SETRA: France) (also available in English).

Hikami, Y. and Shiraishi, N., Rain-induced vibrations of cables in cable-stayed bridges. *J. Wind Engng Indust. Aerodyn.*, 1988, **29**, 409–418.

Irvine, M., *Cable Structures*, 1981 (MIT Press: Cambridge, MA).

Irwin, P.A., Wind vibrations of cables on cable-stayed bridges, in *Proceedings of the ASCE Structure Congress*, Portland, Oregon, 14–16 April, 1997.

Kovacs, I., Zur Frage der Seilschwingungen und der Seildampfung. *Die Bautechnik*, 1982, October, 325–332.

Kwork, K.C.F. and Wong, C.K.P., The choice, design and testing of stay cables of Stonecutters Bridge, in *Proceedings of the Shanghai IABSE Symposium*, 2004 (CD-Rom).

Main, J.A. and Jones, N.P., Full-scale measurements of stay cable vibration. In *Wind Engineering into the 21st Century*, edited by Larsen, Larose and Livesey, pp. 963–970, 1999 (Balkema: Rotterdam).

Matsumoto, M., Hikami, Y. and Mitazava, M., Cable vibration and its aerodynamic/mechanical control, in *Proceedings of the International Conference on Cable-stayed and Suspension Bridges (AFPC)*, Deauville, 1994, Volume 2, pp. 439–452.

Matsumoto, M., Knisely, C.W., Shiraishi, N. and Saito, T., Inclined cable aerodynamics, in *Proceedings of the ASCE Structures Congress*, San Francisco, 1989, pp. 81–90.

Matsumoto, M., Yagi, T. and Tsushima, D., Inclined cable aerodynamics. Velocity restricted response at high reduced velocity, in *Third International Symposium on Cable Dynamics,* Trondheim, 16–18 August 1999. Proceedings, pp. 91–96.

Matsumoto, M., Yokohama, K., Miyata, T., Fujino, Y. and Yamaguchi, H., Wind-induced cable vibration of cable-stayed bridges in Japan, in *Proceedings of the Canada–Japan Workshop on Bridge Aerodynamics*, Ottawa, September 1989, pp. 101–110.

Miyata, T., Design consideration for wind effects on long span cable-stayed bridges. In *Cable-stayed Bridges. Recent Developments and Their Future*, edited by M. Ito *et al.*, pp. 235–255, 1991 (Elsevier: Amsterdam).

Miyata, T., Yamada, H. and Hojo, T., Aerodynamic response of PE stay cables with pattern-indented surface, in *Proceedings of the International Conference on Cable-stayed and Suspension Bridges (AFPC)*, Deauville, 1994, Volume 2, pp. 515–522.

Morisset, A. and Riché, Ch., Les calculs en grands déplacements du Pont de Normandie. *Annales de l'ITBTP*, 1994, Octobre, 64–84.

PTI., *Recommendations for Stay Cable Design, Testing and Installations*, fourth edition, February 2001 (Post-Tensioning Institute: USA).

Recommendation for acceptance of stay cable systems using prestressing steel. Fédération Internationale du Béton. Fib, Lausanne, January 2005.

Saito, T., Matsumoto, M. and Kitazawa, M., Rain-wind excitation of cables on cable-stayed Higashi-Kobe bridge and cable vibration control, in *Proceedings of the International Conference on Cable-stayed and Suspension Bridges (AFPC)*, Deauville, 1994, Volume 2, pp. 507–510.

Simiu, E. and Scanlan, R., *Wind Effects on Structures*, third edition, 1996 (John Wiley and Sons: New York).

Virlogeux, M., Wind design and analysis for the Normandie Bridge. In *Aerodynamics of Large Bridges*, edited by A. Larsen, pp. 183–216, 1992 (Balkema: The Netherlands).

Virlogeux, M., Design of cables for cable-stayed bridges: the example of the Normandie Bridge, in *International Conference on Cable Vibration, Liège*, October 1996. Addendum to the proceedings, pp. 13–31.

Virlogeux, M., Cable vibrations in cable-stayed bridges, in *International Symposium on Advances in Bridge Aerodynamics*, Copenhagen, 1998a, edited by A. Larsen and S. Esdahl, pp. 213–233 (Balkema: The Netherlands).

Virlogeux, M., *Design of cables for cable-stayed bridges: the example of the Normandie Bridge. The French Technology of Concrete*. Special publication for the FIP congress in Amsterdam, 1998b (AFPC: Bagneux).

Yamaguchi, H., Analytical study on growth mechanism of rain vibration of cables. *J. Wind Engng Indust. Aerodyn.,* 1990, **33**, 73–80.

Yamaguchi, H. and Fujino, Y., Damping of cables in cable-stayed bridges with and without vibration. Control measures, in *Proceedings of the International Conference on Cable-stayed and Suspension Bridges (AFPC)*, Deauville, 1994, Volume 2.